

***H*-theorem and boundary conditions for two-temperature model: Application to wave propagation and heat transfer in polyatomic gases**

Anil Kumar^{*} and Anirudh Singh Rana[†]*Department of Mathematics, Birla Institute of Technology and Science, Pilani, Rajasthan 333031, India*

(Received 8 August 2023; accepted 16 October 2023; published 7 December 2023)

Polyatomic gases find numerous applications across various scientific and technological fields, necessitating a quantitative understanding of their behavior in nonequilibrium conditions. In this study, we investigate the behavior of rarefied polyatomic gases, particularly focusing on heat transfer and sound propagation phenomena. By utilizing a two-temperature model, we establish constitutive equations for internal and translational heat fluxes based on the second law of thermodynamics. A novel *reduced two-temperature model* is proposed, which accurately describes the system's behavior while reducing computational complexity. Additionally, we develop phenomenological boundary conditions adhering to the second law, enabling the simulation of gas-surface interactions. The phenomenological coefficients in the constitutive equations and boundary conditions are determined by comparison with relevant literature. Our computational analysis includes conductive heat transfer between parallel plates, examination of sound wave behavior, and exploration of spontaneous Rayleigh-Brillouin scattering. The results provide valuable insights into the dynamics of polyatomic gases, contributing to various technological applications involving heat transfer and sound propagation.

DOI: [10.1103/PhysRevE.108.065103](https://doi.org/10.1103/PhysRevE.108.065103)

I. INTRODUCTION

Polyatomic gases have a plethora of applications that span across various fields of science and technology, ranging from aeronautics and astronautics to plasma physics and energy production. Understanding these phenomena in a quantitative and reliable manner is essential, as they present stimulating yet challenging scientific problems that garner significant research interest. Moreover, this understanding extends beyond gas flows, as demonstrated by the blue color of the sky and the red appearance of the moon during a lunar eclipse. These phenomena are attributed to Rayleigh scattering, occurring when particles in the atmosphere are smaller than the wavelength of light [1]. Nitrogen and oxygen molecules, abundant in the Earth's atmosphere, play a major role in Rayleigh scattering. Investigating these scattering processes not only enhances our understanding of various atmospheric behaviors but also sheds light on optical phenomena influencing our environment.

The intricate molecular structures found in polyatomic gases have a significant impact on the scattering of light and the resulting color observed. When designing gas sensors to detect and measure these types of gases effectively, it is essential to consider the strong nonequilibrium effects. This includes considering the limit of a large Knudsen number, Kn , which is determined by the ratio of the mean free path (λ) in the gas to a characteristic length scale (L) of the flow. Additionally, it is important to consider a large Weissenberg number [2], which relates to the relaxation time that character-

izes the rate at which perturbations in the gas decay in relation to the characteristic time scale of the system, such as the inverse frequency of light or the sound wave. In particular, in polyatomic gases, another mechanism responsible for deviation from equilibrium is the finite rate of relaxation of internal degrees of freedom with random translational energy, which leads to a large ratio of bulk viscosity to shear viscosity. While the classical Navier-Stokes-Fourier (NSF) equations are applicable when the ratio of bulk viscosity to shear viscosity is small, gases such as CH_4 , CO_2 , and H_2 exhibit significantly large ratios [3,4], rendering the one-temperature model is inadequate [5]. In such cases, the two-temperature model becomes essential for accurately capturing the system's behavior [6–8].

In recent literature, several sets of equations for the two-temperature model have been proposed and studied. Notably, the two-temperature Navier-Stokes equations derived from an ellipsoidal Bhatnagar-Gross-Krook (ES-BGK) model for a polyatomic gas have been studied [9]. These investigations focus on regimes where the bulk viscosity significantly exceeds the shear viscosity and are based on a discrete structure of internal energy levels [5,10]. In the current study, we concentrate on determining the nonequilibrium distribution function using the maximum entropy principle [11] and establishing the second law of thermodynamics for the two-temperature model. The phenomenological coefficients are determined by comparing different collision models found in the literature.

In the field of nonequilibrium thermodynamics, various approaches exist to determine the behavior of a system near equilibrium. One approach is linear irreversible thermodynamics (LIT) [12], which assumes local thermodynamic equilibrium and derives constitutive laws for the stress tensor and heat flux based on the second law of thermodynamics.

^{*}p20200044@pilani.bits-pilani.ac.in[†]anirudh.rana@pilani.bits-pilani.ac.in; <https://www.bits-pilani.ac.in/pilani/anirudhrana/profile>

However, rational extended thermodynamics (RET) relaxes the requirement of local thermodynamic equilibrium by introducing the Clausius-Duhem equation as a specific form of entropy balance law [13]. Despite their differing postulates, RET [7,14] and LIT, two thermodynamic approaches, yield equivalent constitutive equations for simple fluids, including those governing local thermodynamic equilibrium [13,15]. An important feature of both approaches is that the entropy generation rate is expressed as the sum of products of thermodynamic forces and thermodynamic fluxes. The formulation begins by establishing an extended Gibbs equation and applying the second law of thermodynamics to ensure a positive entropy generation rate.

While thermodynamics, including both rational and extended versions, is commonly employed to investigate these phenomena, the molecular dynamics or kinetic approach [16–18] provides deeper insights, although it comes with the drawback of large computational costs. As a result, in many cases, it becomes desirable to utilize simpler macroscopic models, known as extended hydrodynamics models, which prove highly valuable for engineering purposes. Rahimi and Struchtrup [19] have developed a kinetic model and a high-order macroscopic model to accurately represent rarefied polyatomic gas flows at moderate Knudsen numbers. The kinetic model extends the Shakov model (S-model) [20,21] and accurately captures the dynamics of higher moments. Through the order of magnitude method [22,23], optimized moment definitions and scaled Grad's 36-moment equations are obtained. The first order yields a modified version of the Navier-Stokes-Fourier equations, while the third-order results in a set of 19 regularized partial differential equations (R19). Aoki *et al.* [9] investigated a polyatomic gas with slow relaxation of internal modes and derived the Navier-Stokes equations with two temperatures (translational and internal temperatures) based on the ellipsoidal-statistical (ES) model of the Boltzmann equation proposed by Andries *et al.* [24]. The derivation was carried out using the Chapman-Enskog procedure. Djordjić *et al.* [25] developed collision kernel models and used the nonlinear Boltzmann collision operator for polyatomic gases to derive explicit expressions for transport coefficients, including shear and bulk viscosities and thermal conductivity. These coefficients depend on the parameters of the collision kernel. Marques and Kremer [26] proposed a hydrodynamical model that incorporates a relaxation equation for dynamic pressure into the conventional hydrodynamic equations based on the field equations of a polyatomic gas consisting of rough spherical molecules [27].

In this article, we first establish the second law for the two-temperature model by deriving the extended Gibbs equation from the maximum entropy distribution, incorporating six field variables, namely, density, momentum, translational temperature, and internal temperature. Furthermore, we derive constitutive equations for internal heat flux (q_k^i) and translational heat flux (q_k^m) based on the second law. Additionally, drawing inspiration from the order of magnitude technique [22,23], we reformulate the internal and translational heat fluxes as the summation of the total heat flux (q_k) and additional heat flux (Q_k), with the magnitude of Q_k being larger than that of the total heat flux [19]. Thus, to achieve the desired accuracy for the first order, we determine

the phenomenological coefficients such that the impact of the additional heat flux vanishes. This approach is referred to as the “reduced two-temperature model,” where the relevant field variables include mass momentum and two temperatures, while the constitutive relationships are established for stress and the total heat flux. To assess the validity and scope of the two-temperature model equation, we examine its performance in analyzing time-dependent phenomena such as sound propagation and light scattering in dilute polyatomic gases. By comparing our theoretical predictions to experimental data, including acoustic measurements in nitrogen and oxygen by Greenspan [28], and the extended hydrodynamic theory of Hammond and Wiggins [29] in methane, we demonstrate that the proposed model equation effectively describes the acoustic properties and light-scattering spectrum of dilute polyatomic gases.

Boundary conditions play a crucial role in gas dynamics simulations as they define the behavior of the fluid at the boundaries, describing how the gas interacts with solid surfaces. This includes various phenomena, such as momentum and heat transfer, chemical reactions, and phase change. The selection of suitable boundary conditions significantly impacts the accuracy and reliability of simulation outcomes. In this study, our objective is to derive phenomenological boundary conditions (PBCs) specifically for the two-temperature model applied to polyatomic gases.

To establish these PBCs, we employ an entropy balance integrated around the interface between the solid and gas. The PBCs are developed as empirical rules to ensure a positive entropy inequality at the boundary and to represent the entropy generation at the boundary using these relations. These PBCs can be employed to solve boundary value problems. In a recent work by [30], the authors proposed phenomenological boundary conditions for the linearized R13 equation using the second law of thermodynamics. They evaluated the phenomenological coefficients by comparing slip/jump and thermal creep coefficients with the linearized Boltzmann equation for different accommodation coefficients. Similarly, in a set of phenomenological boundary conditions was proposed for a coupled constitutive relation [31,32]. These conditions were designed to uphold the second law of thermodynamics, a fundamental principle in physics governing the behavior of energy and heat.

Kosuge *et al.* [33] developed slip boundary conditions for the two-temperature system with a polyatomic gas, utilizing the ES model and incorporating the Maxwell-type diffuse-specular reflection condition on the boundary. Rahimi and Struchtrup [19] introduced a kinetic boundary condition that incorporates the concept of two distinct exchanging processes: translational and internal. They utilize this condition to derive appropriate macroscopic boundary conditions.

For both the two-temperature model and the reduced two-temperature model, this article establishes a set of wall boundary conditions adhering to the second law of thermodynamics. The phenomenological coefficients appearing in the boundary conditions are calculated by comparing them with kinetic theory in the asymptotic limit of small dynamic temperature (ϑ) [19].

This study analyzes conductive heat transfer in rarefied polyatomic gases confined between parallel plates.

Furthermore, we examine the behavior of sound waves in rarefied polyatomic gases, with a specific focus on nitrogen and hydrogen gases. Additionally, we explore the occurrence of spontaneous Rayleigh-Brillouin scattering. The exact investigation of the Rayleigh-Brillouin spectral line shape is of practical importance as it provides valuable information about the velocity, density, and temperature of gas samples when illuminated. Heat transfer configurations play a critical role in various technological applications, including vacuum pressure gauges [34], vacuum solar collectors [35], multilayer insulation blankets used in space and cryogenic equipment [36], as well as micro heat exchangers and microsensors [37,38]. Furthermore, these configurations serve as standard setups for determining important properties such as the thermal conductivity of gases [39], temperature jump coefficient [40], and energy accommodation at different surface temperatures [41]. These evaluations involve a combination of modeling and experimental measurements [42,43].

The remaining sections of the paper are organized as follows: In Sec. II, we establish the definitions of moments and derive the conservation laws and extended balance equations from the Boltzmann equation. In Sec. III, we focus on determining the nonequilibrium distribution function by applying the maximum entropy principle and proving the second law of thermodynamics. Additionally, we derive constitutive relations for the two-temperature model and determine the values of phenomenological coefficients. Subsequently, we discuss linearized and dimensionless equations and introduce a reduced model in Secs. IV and V, respectively. In Sec. VI, we conduct a linear stability analysis for different values of phenomenological coefficients. Furthermore, we analyze sound wave propagation in Sec. VII and explore the problems of spontaneous Rayleigh-Brillouin scattering in Sec. VIII. Determining the appropriate wall boundary conditions for the two-temperature model using the second law of thermodynamics is addressed in Sec. IX. We validate the above wall boundary conditions through an investigation of the fundamental problem of heat transfer between two parallel plates in Sec. X. Finally, in Sec. XI, we present our concluding remarks.

II. MOMENT SYSTEM

The Boltzmann equation provides a kinetic description of polyatomic gases via the one-body distribution function $f(t, \mathbf{x}, \mathbf{c}, I)$ which can be formally written as [7]

$$\frac{\partial f}{\partial t} + c_k \frac{\partial f}{\partial x_k} + F_k \frac{\partial f}{\partial c_k} = \mathcal{S}[f, f]. \quad (1)$$

The distribution function $f(t, \mathbf{x}, \mathbf{c}, I)$ describes the state of the gas molecules having three translational degrees of freedom and internal degrees of freedom, where $t \in \mathbb{R}^+$ is the time, $\mathbf{x} \in \mathbb{R}^3$ is the spatial position, $\mathbf{c} \in \mathbb{R}^3$ is the molecular translational velocity, F_k is the field of the external forces, e.g., gravity, and I denotes the specific energy of a gas molecule due to internal modes with $I \in \mathbb{R}^+$. The right-hand side of Eq. (1) is known as the collision operator, which represents the rate of change in f due to binary collisions. The collision operator in Eq. (1) involves complex integrals whose actual form depends on the detailed nature of the intermolecular interactions. Fur-

thermore, the binary collision operator \mathcal{S} have five collision invariants: mass, three components of momentum, and energy, given by

$$\psi = m \left\{ 1, c_i, \frac{C^2}{2} + I \right\}, \quad (2)$$

i.e., $\int \mathcal{S} \psi d\mathbf{c} dI = 0$.

The macroscopic variables, namely local density ρ , momentum density ρv_i , and internal energy u , can be defined as the moment of the distribution function as

$$\rho = m \int f d\mathbf{c} dI, \quad \rho v_i = m \int f c_i d\mathbf{c} dI, \quad (3)$$

$$\rho u = m \int f \left(\frac{C^2}{2} + I \right) d\mathbf{c} dI, \quad (4)$$

where m is the molecular mass, and $\mathbf{C} = \mathbf{c} - \mathbf{v}$ is the peculiar velocity with respect to the macroscopic velocity \mathbf{v} (or v_i in tensorial notation). The differential velocity vector $d\mathbf{c}$ implies integration over all three components of velocity space. Furthermore, the internal energy u can be divided into the translational part u^{tr} and the part due to the internal degrees of freedom u^{in} , as

$$\rho u^{\text{tr}} := \frac{3}{2} \rho \theta^{\text{tr}} = m \int f \frac{C^2}{2} d\mathbf{c} dI, \quad (5)$$

$$\rho u^{\text{in}} := \frac{\delta}{2} \rho \theta^{\text{in}} = m \int f I d\mathbf{c} dI. \quad (6)$$

Here, superscripts “tr” and “in” denote the translational and internal parts, while the parameter δ is the number of internal degrees of freedom. Conventionally, we define the translational temperature θ^{tr} and the internal temperature θ^{in} in energy units. As a result, the thermodynamic temperature θ (defined as $\theta := RT$; R being the gas constant) can be expressed as follows:

$$\frac{3 + \delta}{2} \theta = \frac{3}{2} \theta^{\text{tr}} + \frac{\delta}{2} \theta^{\text{in}}. \quad (7)$$

When the system is in equilibrium, the three temperatures are equal: $\theta^{\text{tr}} = \theta^{\text{in}} = \theta$. However, in a nonequilibrium state, these temperatures can differ. To quantify the nonequilibrium part of the temperature, we introduce the dynamic temperature denoted as $\vartheta = \theta^{\text{tr}} - \theta$. In this context, the dynamic pressure in the gas can be expressed as $\Pi = \rho \vartheta$.

The pressure tensor p_{ij} is defined as follows:

$$p_{ij} = m \int f c_i c_j d\mathbf{c} dI, \quad (8)$$

so that its trace $p_{kk} = 3\rho\theta^{\text{tr}}$. Furthermore, the pressure tensor is expressed in terms of its trace and traceless part as

$$p_{ij} = (p + \Pi)\delta_{ij} + \sigma_{(ij)}, \quad (9)$$

where δ_{ij} is the Kronecker δ function, the angular brackets around indices represent the symmetric and traceless part of a tensor, p is the equilibrium pressure, σ_{ij} is the viscous stress tensor, and Π is the dynamic pressure (or nonequilibrium pressure). We can further define the translational heat flux and

internal heat flux as

$$q_k^{\text{in}} := m \int f I C_k d\mathbf{c} dI, \quad (10)$$

$$q_k^{\text{tr}} := m \int f \frac{C^2}{2} C_k d\mathbf{c} dI. \quad (11)$$

Furthermore, the total heat flux q_k and the heat flux difference Q_k are introduced as moments of the distribution functions. They are defined as follows:

$$q_k := m \int f \left(\frac{C^2}{2} + I \right) C_k d\mathbf{c} dI = q_k^{\text{tr}} + q_k^{\text{in}}, \quad (12)$$

$$Q_k := q_k^{\text{tr}} - \frac{5\theta + 3\vartheta}{\delta\theta - 3\vartheta} q_k^{\text{in}}. \quad (13)$$

The idea behind selecting a particular expression for Q_k was motivated by the order-of-magnitude approach proposed by Rahimi and Struchtrup [19]. This approach revealed that the magnitude of this term can be approximated as $O(\text{Kn}^{1+\alpha})$, where α is a magnification parameter falling within the range of 0 to 1. Furthermore, opting for a specific combination of q_k^{tr} and q_k^{in} in a linear fashion results in a convenient expression for the entropy flux, which will be further discussed in Sec. III.

A. The conservation laws and extended balance equations

The conservation laws are obtained from the Boltzmann equation (1), by multiplying it with the collision invariants (2) and integrating, to get

$$\frac{D\rho}{Dt} + \rho \frac{\partial v_k}{\partial x_k} = 0, \quad (14a)$$

$$\rho \frac{Dv_i}{Dt} + \frac{\partial p_{ik}}{\partial x_k} = 0, \quad (14b)$$

$$\rho \frac{D \frac{3+\delta}{2} \theta}{Dt} + p_{ik} \frac{\partial v_i}{\partial x_k} + \frac{\partial q_k}{\partial x_k} = 0. \quad (14c)$$

Here, $\frac{D}{Dt} = \frac{\partial}{\partial t} + v_k \frac{\partial}{\partial x_k}$ is the convective time derivative. We also get the balance equations for the translational temperature and internal temperature as follows:

$$\rho \frac{3}{2} \frac{D\theta^{\text{tr}}}{Dt} + p_{ik} \frac{\partial v_i}{\partial x_k} + \frac{\partial q_k^{\text{tr}}}{\partial x_k} = \mathcal{P}^{0,0}, \quad (15)$$

$$\rho \frac{\delta}{2} \frac{D\theta^{\text{in}}}{Dt} + \frac{\partial q_k^{\text{in}}}{\partial x_k} = \mathcal{P}^{0,1}. \quad (16)$$

The production terms $\mathcal{P}^{0,0}$ and $\mathcal{P}^{0,1}$ are obtained from the Boltzmann collision operator, which entails that

$$\mathcal{P}^{0,0} := m \int \mathcal{L} \frac{C^2}{2} d\mathbf{c} dI, \quad \text{and} \quad \mathcal{P}^{0,1} := m \int \mathcal{L} I d\mathbf{c} dI,$$

therefore $\mathcal{P}^{0,0} = -\mathcal{P}^{0,1}$, since $\frac{C^2}{2} + I$ is collision invariant. Further, the balance law for dynamic temperature is written as

$$\frac{3\rho}{2} \frac{D\vartheta}{Dt} + \frac{\delta}{3+\delta} p_{ik} \frac{\partial v_i}{\partial x_k} - \frac{3}{3+\delta} \frac{\partial q_k}{\partial x_k} + \frac{\partial q_k^{\text{tr}}}{\partial x_k} = \mathcal{P}^{0,0}. \quad (17)$$

In terms of total heat and heat difference flux, the last equation can also be written as

$$\begin{aligned} & \frac{3\rho}{2} \frac{D\vartheta}{Dt} + \frac{\delta}{3+\delta} p_{ik} \frac{\partial v_i}{\partial x_k} + \frac{2}{5+\delta} \left(\frac{\delta}{3+\delta} + \frac{3}{2} \frac{\vartheta}{\theta} \right) \frac{\partial q_k}{\partial x_k} \\ & + \frac{3}{5+\delta} q_k \frac{\partial}{\partial x_k} \left(\frac{\vartheta}{\theta} \right) + \frac{\delta}{5+\delta} \left(1 - \frac{3}{\delta} \frac{\vartheta}{\theta} \right) \frac{\partial Q_k}{\partial x_k} \\ & - \frac{3}{5+\delta} Q_k \frac{\partial}{\partial x_k} \left(\frac{\vartheta}{\theta} \right) = \mathcal{P}^{0,0}. \end{aligned} \quad (18)$$

The governing equations (14) and (15) describe flow behavior but require additional closure models to relate unknown fluxes $\{\sigma_{ij}, q_k^{\text{tr}}, q_k^{\text{in}}\}$ to known quantities $\{\rho, v_i, \theta^{\text{tr}}, \theta^{\text{in}}\}$.

III. SECOND LAW OF THERMODYNAMICS

This section focuses on obtaining the nonequilibrium distribution function f_6 by applying the maximum entropy principle. Additionally, the second law of thermodynamics is proven, and constitutive relations are derived. The constitutive relations are functional relations between the dependent fields $\{\sigma_{ij}, q_k^{\text{tr}}, q_k^{\text{in}}\}$ and the independent fields $\{\rho, v_i, \theta^{\text{tr}}, \theta^{\text{in}}\}$ that is we expressed independent field variables as functional relations of dependent field variables.

The second law of thermodynamics asserts that a physical system in equilibrium has maximal entropy among all states with the same energy. The second law of thermodynamics, which we now introduce in the form of the entropy principle. The entropy principle will always be exploited for supply-free bodies, i.e., there are no body forces and no radiation, nor is there a supply of entropy. There exists a specific entropy of the gas s , the nonconvective entropy flux h_k , and entropy production density Σ , which obey a balance law.

The entropy density is defined by the relation

$$\rho s = -k_b \int f \ln \frac{f}{f_0} d\mathbf{c} dI, \quad (19)$$

and the entropy law

$$\rho \frac{Ds}{Dt} + \frac{\partial h_k}{\partial x_k} = \Sigma, \quad (20)$$

where k_b is the Boltzmann constant, Σ the entropy production and $f_0 = I^{(\frac{\delta}{2}-1)}$. The second law of thermodynamics requires entropy production density nonnegative, i.e., $\Sigma \geq 0$. Now, any process satisfying the second law represents a so-called physically admissible process. The density of entropy production is nonnegative for all thermodynamic processes, i.e., for all solutions of the field equations. Thus, the entropy inequality ($\Sigma \geq 0$) holds for all thermodynamic processes. First of all, we determine the phase density f_6 that maximizes the entropy density ρs under the constraints of fixed mass density ρ , momentum density ρv_i and internal energy density ρu (both parts). After that, we introduce it into the expressions (19) to obtain the entropy density.

Theorem 1. The maximum entropy distribution function which maximizes the entropy (19) under the

constraints (3), (5), and (6) takes the following form [44]:

$$f_6 = \frac{\rho}{m} \underbrace{\frac{1}{(2\pi\theta^{\text{tr}})^{3/2}} e^{-\frac{c^2}{2\theta^{\text{tr}}}}}_{\text{Maxwellian}} \underbrace{\frac{1}{\gamma\left(\frac{\delta}{2}\right)} \frac{1}{I} \left(\frac{I}{\theta^{\text{in}}}\right)^{\delta/2}}_{\text{Gamma}} e^{-\frac{I}{\theta^{\text{in}}}}.$$

Proof. See Appendix. ■

Therefore, the entropy density for the six-moment system is given by the relation

$$\rho s = -k_b \int f_6 \ln\left(\frac{f_6}{f_0}\right) d\mathbf{c} dI = \rho \left\{ \frac{3}{2} \ln \theta^{\text{tr}} + \frac{\delta}{2} \ln \theta^{\text{in}} - \ln \rho \right\}. \tag{21}$$

Moreover, The extended Gibbs' relation is given by

$$\rho ds = \frac{3}{2\theta^{\text{tr}}} \rho d\theta^{\text{tr}} + \frac{\delta}{2\theta^{\text{in}}} \rho d\theta^{\text{in}} - d\rho. \tag{22}$$

The proof for Eqs. (21) and (22) is simple and straightforward. Gibbs' relation can be obtained by differentiating equation (21). Now, using the extended Gibbs equation (22), the time rate of change of the entropy of a material element is given as

$$\rho \frac{Ds}{Dt} = \frac{3}{2\theta^{\text{tr}}} \rho \frac{D\theta^{\text{tr}}}{Dt} + \frac{\delta}{2\theta^{\text{in}}} \rho \frac{D\theta^{\text{in}}}{Dt} - \frac{D\rho}{Dt}. \tag{23}$$

Using Eqs. (14a), (15), and (16) in Eq. (23), we get

$$\begin{aligned} \rho \frac{Ds}{Dt} + \frac{\partial\left(\frac{q_k^{\text{tr}}}{\theta^{\text{tr}}} + \frac{q_k^{\text{in}}}{\theta^{\text{in}}}\right)}{\partial x_k} \\ = -\frac{1}{\theta^{\text{tr}}} \sigma_{ik} \frac{\partial v_i}{\partial x_k} + q_k^{\text{tr}} \frac{\partial\left(\frac{1}{\theta^{\text{tr}}}\right)}{\partial x_k} \\ + q_k^{\text{in}} \frac{\partial\left(\frac{1}{\theta^{\text{in}}}\right)}{\partial x_k} + \left(\frac{1}{\theta^{\text{in}}} - \frac{1}{\theta^{\text{tr}}}\right) \mathcal{P}^{0,1}. \end{aligned} \tag{24}$$

Comparing the above equation with the entropy law (20), we identify the nonconvective entropy flux h_k as follows:

$$h_k = \frac{q_k^{\text{tr}}}{\theta^{\text{tr}}} + \frac{q_k^{\text{in}}}{\theta^{\text{in}}}. \tag{25}$$

Clearly, when the system is in equilibrium ($\theta^{\text{tr}} = \theta^{\text{in}} = \theta$), the three temperatures are equal, and the above expression simplifies to the classical entropy flux expression, i.e., $h_k = q_k/\theta$.

By introducing the variables q_k , Q_k , θ , and ϑ , Eq. (25) can be rewritten as follows:

$$h_k = \frac{q_k}{\theta} - \frac{2}{5 + \delta} \frac{\vartheta}{\theta(\theta + \vartheta)} q_k - \frac{3 + \delta}{5 + \delta} \frac{\vartheta}{\theta(\theta + \vartheta)} Q_k. \tag{26}$$

Indeed, in Eq. (13), we have introduced Q_k so that entropy flux can be conveniently decomposed into three components. The first contribution to the entropy flux is classical, the second one stems from coupled constitutive relations [45], whereas the last is the contribution of higher order. Furthermore, via order of magnitude analysis, it can be shown that the first term is of the order $O(\text{Kn}^1)$ the second term is of the order $O(\text{Kn}^{1+\alpha})$, and the third term is of the order $O(\text{Kn}^{1+2\alpha})$.

Again, comparing Eq. (20) with the entropy law (20), we get the entropy production rate, as

$$\begin{aligned} \Sigma = -\frac{1}{\theta^{\text{tr}}} \sigma_{ik} \frac{\partial v_i}{\partial x_k} - \frac{1}{\theta^{\text{tr}2}} q_k^{\text{tr}} \frac{\partial \theta^{\text{tr}}}{\partial x_k} - \frac{1}{\theta^{\text{in}2}} q_k^{\text{in}} \frac{\partial \theta^{\text{in}}}{\partial x_k} \\ + \left(\frac{1}{\theta^{\text{in}}} - \frac{1}{\theta^{\text{tr}}}\right) \mathcal{P}^{0,1}, \end{aligned} \tag{27}$$

which is in the bilinear form for flux and gradients. The second law of thermodynamics requires that the entropy production rate must be positive, i.e., $\Sigma \geq 0$. To ensure the positivity of the entropy production rate Σ , it is sufficient to assume relations of the form

$$\sigma_{ik} = -2\mu \frac{\partial v_{\langle i}}{\partial x_k \rangle}, \tag{28a}$$

$$q_k^{\text{tr}} = -\zeta_{11} \frac{1}{\theta^{\text{tr}2}} \frac{\partial \theta^{\text{tr}}}{\partial x_k} - \zeta_{12} \frac{1}{\theta^{\text{in}2}} \frac{\partial \theta^{\text{in}}}{\partial x_k}, \quad \text{and} \tag{28b}$$

$$q_k^{\text{in}} = -\zeta_{12} \frac{1}{\theta^{\text{tr}2}} \frac{\partial \theta^{\text{tr}}}{\partial x_k} - \zeta_{22} \frac{1}{\theta^{\text{in}2}} \frac{\partial \theta^{\text{in}}}{\partial x_k}, \tag{28c}$$

where $\mu \geq 0$ is viscosity of the gas and the matrices

$$\eta = \begin{bmatrix} \zeta_{11} & \zeta_{12} \\ \zeta_{12} & \zeta_{22} \end{bmatrix} \tag{29}$$

is a symmetric nonnegative definite matrix.

One can express the total heat flux (q_k) and the heat difference (Q_k), using Eqs. (28b) and (28c),

$$q_k = -\left[\frac{\zeta_{11} + \zeta_{12}}{(\theta + \vartheta)^2} + \frac{(\zeta_{12} + \zeta_{22})\delta^2}{(\delta\theta - 3\vartheta)^2} \right] \frac{\partial \theta}{\partial x_k} - \left[\frac{\zeta_{11} + \zeta_{12}}{(\theta + \vartheta)^2} - \frac{3(\zeta_{12} + \zeta_{22})\delta}{(\delta\theta - 3\vartheta)^2} \right] \frac{\partial \vartheta}{\partial x_k}, \quad \text{and} \tag{30}$$

$$\begin{aligned} Q_k = -\left[\frac{\zeta_{11}}{(\theta + \vartheta)^2} - \frac{\zeta_{22}(5\theta + 3\vartheta)\delta^2}{(\delta\theta - 3\vartheta)^3} - \frac{\zeta_{12}\{-\delta^2(\theta + \vartheta)^2 + \delta\theta(5\theta + 3\vartheta) - 3\vartheta(5\theta + 3\vartheta)\}}{(\theta + \vartheta)^2(\delta\theta - 3\vartheta)^2} \right] \frac{\partial \theta}{\partial x_k} \\ - \left[\frac{\zeta_{11}}{(\theta + \vartheta)^2} + \frac{3\zeta_{22}(5\theta + 3\vartheta)\delta}{(\delta\theta - 3\vartheta)^3} - \frac{\zeta_{12}\{8\delta\theta^2 + 3(-5 + 3\delta)\theta\vartheta + 3(-3 + \delta)\vartheta^2\}}{(\theta + \vartheta)^2(\delta\theta - 3\vartheta)^2} \right] \frac{\partial \vartheta}{\partial x_k}. \end{aligned} \tag{31}$$

Furthermore, one can show that the last term in Eq. (25) is positive, if we take $\mathcal{P}^{0,1}$ to be proportional to ϑ , as

$$\left[\frac{1}{\theta^{\text{in}}} - \frac{1}{\theta^{\text{tr}}} \right] \mathcal{P}^{0,1} = \left[\frac{\theta^{\text{tr}} - \theta^{\text{in}}}{\theta^{\text{tr}}\theta^{\text{in}}} \right] \frac{\rho\vartheta}{\tau_{\text{int}}} = \frac{\rho}{\tau_{\text{int}}} \left[\frac{\theta^{\text{tr}} - \theta^{\text{in}}}{\theta^{\text{tr}}\theta^{\text{in}}} \right] (\theta^{\text{tr}} - \theta) = \frac{\rho\delta}{\tau_{\text{int}}(3 + \delta)} \left[\frac{(\theta^{\text{tr}} - \theta^{\text{in}})^2}{\theta^{\text{tr}}\theta^{\text{in}}} \right] \geq 0, \tag{32}$$

where $\tau_{\text{int}} > 0$ is the relaxation time for ϑ . This completes the proof of H -theorem (second law of thermodynamics) for the two-temperature model.

A. Determination of phenomenological coefficients

In this section, we find the value of arbitrary nonnegative coefficients μ , ζ_{11} , ζ_{22} , ζ_{12} and production terms $\mathcal{P}^{0,1}$ via comparison with different models from literature. The values for these phenomenological coefficients and production terms may vary with different collision models. Here, we consider four models which give different values.

1. Comparison with Marques and Kremer [26] for $\delta = 3$ (Model 1)

Marques and Kremer [26] introduced a hydrodynamical model that includes a relaxation equation for the dynamic pressure, which is the nonequilibrium component of the pressure, in addition to the conventional hydrodynamic equations. We compare proposed model balance equations and constitutive relations with hydrodynamical model [26] equations; we get nonnegative coefficients and production terms as

$$\mu = \frac{15}{8a^2} \left(\frac{k_b \theta m}{\pi} \right)^{1/2} \frac{(\kappa + 1)^2}{(13\kappa + 6)}, \quad (33a)$$

$$\zeta_{11} = \frac{15\mu(6 + 25\kappa + 38\kappa^2 + 26\kappa^3)}{24 + 150\kappa + 202\kappa^2 + 204\kappa^3}, \quad (33b)$$

$$\zeta_{12} = \frac{15\kappa(6 + 13\kappa)\mu}{24 + 150\kappa + 202\kappa^2 + 204\kappa^3}, \quad (33c)$$

$$\zeta_{22} = \frac{9(24 + 154\kappa + 221\kappa^2)\mu}{10(12 + 75\kappa + 101\kappa^2 + 102\kappa^3)}, \quad (33d)$$

$$\mathcal{P}^{0,1} = \frac{\delta \rho}{(3 + \delta)\tau_{\text{int}}} (\theta^{\text{tr}} - \theta^{\text{in}}), \quad (33e)$$

where μ is the shear viscosity, ζ_{11} the thermal conductivity for the translational temperature, ζ_{22} the thermal conductivity for the internal temperature,

$$\frac{1}{\tau_{\text{int}}} = \frac{32}{3} a^2 \frac{\rho}{m} \sqrt{\pi \theta} \frac{\kappa}{(1 + \kappa)^2}, \quad (34)$$

is the relaxation frequency of the dynamic pressure, a and $\kappa = \frac{4I}{ma^2}$ are the diameter and the dimensionless moment of inertia of the spherical molecule respectively [46]. The range of $\kappa \in [0, 2/3]$, with 0 denoting no mass distribution on the surface of the molecule and $2/3$ denoting uniform mass distribution.

2. Comparison with Aoki *et al.* [9] (Model 2)

Aoki *et al.* [9] developed the Navier-Stokes equations for a polyatomic gas that exhibits slow relaxation of its internal modes, using the ellipsoidal-statistical model of the Boltzmann equation proposed by Andries *et al.* [24]. This model considers two temperatures, translational and internal, and Aoki *et al.* used the Chapman-Enskog method to derive the equations. On comparing the balance equations and constitutive relations of the proposed model with the equations of the Aoki *et al.* model, we find the nonnegative coefficients and production terms as

$$\mu = \frac{1}{1 - \nu} \frac{\theta^{\text{tr}}}{2\mathcal{A}_c(T)}, \quad (35a)$$

$$\zeta_{11} = \frac{5\mu}{2} \frac{(\theta^{\text{tr}})^3}{\mathcal{A}_c(T)}, \quad (35b)$$

$$\zeta_{12} = 0, \quad (35c)$$

$$\zeta_{22} = \frac{\delta \mu}{2} \frac{(\theta^{\text{in}})^2 \theta^{\text{tr}}}{\mathcal{A}_c(T)}, \quad (35d)$$

$$\mathcal{P}^{0,1} = \frac{3\delta}{2(3 + \delta)} \theta_1 \mathcal{A}_c(T) \rho^2 (\theta^{\text{tr}} - \theta^{\text{in}}), \quad (35e)$$

where $\nu \in [-\frac{1}{2}, 1)$, $\theta_1 \in (0, 1]$ are the constants that adjust the Prandtl number and the bulk viscosity. In addition, $\mathcal{A}_c(T)$ is a function of T such that $\rho \mathcal{A}_c(T)$ is the collision frequency of the gas molecules.

3. Comparison with Djordjić *et al.* [25] (Model 3)

The macroscopic system of 17-moment equations was derived by Djordjić *et al.* [25] from the Boltzmann equation after proposing a collision kernel for polyatomic gases with continuous internal energy. These equations were then used to calculate important transport properties, including shear viscosity, Prandtl number, and the ratio of bulk to shear viscosities. After that, the proposed collision kernel was then employed to compute these transport properties in the polytropic regime for various polyatomic gases. By examining the balance equations and constitutive relations of the proposed model and comparing them to those of the reduced 17-moment system, we identified both the production terms and nonnegative coefficients as

$$\mu = \frac{p}{P_\sigma^0}, \quad (36a)$$

$$\zeta_{11} = \frac{5\mu(\theta^{\text{tr}})^2}{2} \frac{P_s^0}{(P_q^0 P_s^0 - P_q^1 P_s^1)}, \quad (36b)$$

$$\zeta_{12} = -\frac{\delta \mu (\theta^{\text{in}})^2}{2} \frac{P_q^1}{(P_q^0 P_s^0 - P_q^1 P_s^1)}, \quad (36c)$$

$$\zeta_{21} = -\frac{5\mu(\theta^{\text{tr}})^2}{2} \frac{P_s^1}{(P_q^0 P_s^0 - P_q^1 P_s^1)}, \quad (36d)$$

$$\zeta_{22} = \frac{\delta \mu (\theta^{\text{in}})^2}{2} \frac{P_q^0}{(P_q^0 P_s^0 - P_q^1 P_s^1)}, \quad (36e)$$

$$\mathcal{P}^{0,1} = \frac{3\delta \rho}{2(3 + \delta)} (\theta^{\text{tr}} - \theta^{\text{in}}) P_\Pi^0, \quad (36f)$$

where P_q^0 , P_q^1 , P_s^0 , P_s^1 , P_Π^0 , and P_σ^0 are constants that have different values for different gases. These constants can be directly computed using the Mathematica code in Ref. [47]. The phenomenological coefficients ζ_{12} and ζ_{21} are found to be equal value in the linearized constitutive relations for various gases when considering constant P_q^0 , P_q^1 , P_s^0 , P_s^1 , P_Π^0 and P_σ^0 values in Eqs. (36c) and (36d).

4. Comparison with Rahimi and Struchtrup [19] (Model 4)

By comparing the balance equations and constitutive relations of our proposed model with the high-order macroscopic model developed by Rahimi and Struchtrup [19], we identify

$$\left. \begin{aligned} \zeta_{11} &= \frac{5\lambda}{5+\delta} (\theta^{\text{tr}})^2 \\ \zeta_{22} &= \frac{\delta\lambda}{5+\delta} (\theta^{\text{in}})^2 \\ \text{and } \zeta_{12} &= 0 \end{aligned} \right\}, \quad (37)$$

where λ is the thermal conductivity of the gas. Note that in this comparisons, the viscosity μ corresponds to the same value as ours, and the production term $\mathcal{P}^{0,1}$ is defined as in Eq. (36f).

IV. LINEARIZED AND DIMENSIONLESS EQUATIONS

This section considers dimensionless and linearized equations by introducing small perturbations from their values in a reference rest state characterized by a constant pressure p_0 and a constant temperature θ_0 . The relationships between the field variables and their dimensionless deviations (denoted with hat symbols) from the reference rest state are expressed as

$$\begin{aligned} p &= p_0(1 + \hat{p}), \\ \theta &= \theta_0(1 + \hat{\theta}), \\ v_i &= \sqrt{\theta_0} \hat{v}_i, \quad \sigma_{ij} = p_0 \hat{\sigma}_{ij}, \\ q_i &= p_0 \sqrt{\theta_0} \hat{q}_i \quad \text{and} \quad x_i = L \hat{x}_i, \end{aligned} \quad (38)$$

where L is a characteristic length scale. The linearized conservation laws and balance equations are given by

$$\frac{\partial \hat{\rho}}{\partial \hat{t}} + \frac{\partial \hat{v}_i}{\partial \hat{x}_i} = 0, \quad (39a)$$

$$\frac{\partial \hat{v}_i}{\partial \hat{t}} + \frac{\partial \hat{\rho}}{\partial \hat{x}_i} + \frac{\partial \hat{\theta}^{\text{tr}}}{\partial \hat{x}_i} + \frac{\partial \hat{\sigma}_{ij}}{\partial \hat{x}_j} = 0, \quad (39b)$$

$$\frac{3 + \delta}{2} \frac{\partial \hat{\theta}}{\partial \hat{t}} + \frac{\partial \hat{v}_i}{\partial \hat{x}_i} + \frac{\partial \hat{q}_i}{\partial \hat{x}_i} = 0, \quad (39c)$$

$$\frac{3}{2} \frac{\partial \hat{\theta}^{\text{tr}}}{\partial \hat{t}} + \frac{\partial \hat{v}_i}{\partial \hat{x}_i} + \frac{\partial \hat{q}_i^{\text{tr}}}{\partial \hat{x}_i} = \mathcal{P}^{0,0}, \quad (39d)$$

$$\frac{\delta}{2} \frac{\partial \hat{\theta}^{\text{in}}}{\partial \hat{t}} + \frac{\partial \hat{q}_i^{\text{in}}}{\partial \hat{x}_i} = \mathcal{P}^{0,1}, \quad (39e)$$

and the linearized stress, translational, and internal heat fluxes are specified as

$$\hat{\sigma}_{ij} = -2\text{Kn} \frac{\partial \hat{v}_{(i}}{\partial \hat{x}_{j)}}, \quad (40a)$$

$$\hat{q}_i^{\text{tr}} = -\zeta_{11} \frac{\partial \hat{\theta}^{\text{tr}}}{\partial \hat{x}_i} - \zeta_{12} \frac{\partial \hat{\theta}^{\text{in}}}{\partial \hat{x}_i}, \quad \text{and} \quad (40b)$$

$$\hat{q}_i^{\text{in}} = -\zeta_{21} \frac{\partial \hat{\theta}^{\text{tr}}}{\partial \hat{x}_i} - \zeta_{22} \frac{\partial \hat{\theta}^{\text{in}}}{\partial \hat{x}_i}. \quad (40c)$$

Next, we linearized the total heat flux q_k and heat flux difference Q_k ,

$$\begin{aligned} \hat{q}_i &= -(\zeta_{11} + 2\zeta_{12} + \zeta_{22}) \frac{\partial \hat{\theta}}{\partial \hat{x}_i} \\ &\quad - \left((\zeta_{11} + \zeta_{12}) - \frac{3}{\delta} (\zeta_{12} + \zeta_{22}) \right) \frac{\partial \hat{\vartheta}}{\partial \hat{x}_i}, \end{aligned} \quad (41)$$

and

$$\begin{aligned} \hat{Q}_i &= - \left((\zeta_{11} - \frac{5}{\delta} \zeta_{12}) + (\zeta_{12} - \frac{5}{\delta} \zeta_{22}) \right) \frac{\partial \hat{\theta}}{\partial \hat{x}_i} \\ &\quad - \left((\zeta_{11} - \frac{5}{\delta} \zeta_{12}) - \frac{3}{\delta} (\zeta_{12} - \frac{5}{\delta} \zeta_{22}) \right) \frac{\partial \hat{\vartheta}}{\partial \hat{x}_i}. \end{aligned} \quad (42)$$

In Eq. (40), the Knudsen number appears as the scaled viscosity $\text{Kn} = \mu_0 \sqrt{\theta_0} / (p_0 L)$. Henceforward, we removed the hat symbols for better reliability, and all the variables are in dimensionless forms unless otherwise stated.

V. REDUCED MODEL

In this section, we have introduced a reduced model derived from the present two-temperature model. In this simplified model, we assume that the heat fluxes (represented by Q_k) are negligible. This assumption entails setting the coefficients of the gradients of θ and ϑ equal to zero in Eq. (31). By doing so, we solve for ζ_{12} and ζ_{22} in terms of ζ_{11} , and resulting in the following relationships between the phenomenological coefficients,

$$\zeta_{12} = \frac{\delta\theta - 3\vartheta}{5\theta + 3\vartheta} \zeta_{11} \quad \text{and} \quad \zeta_{22} = \frac{(\delta\theta - 3\vartheta)^2}{(5\theta + 3\vartheta)^2} \zeta_{11}. \quad (43)$$

Now, we write linearized reduced model equations in six field variable mass density ρ , velocity v_i , temperature θ , and the dynamic temperature ϑ as

$$\frac{\partial \rho}{\partial t} + \frac{\partial v_i}{\partial x_i} = 0, \quad (44a)$$

$$\frac{\partial v_i}{\partial t} + \frac{\partial \rho}{\partial x_i} + \frac{\partial \theta}{\partial x_i} + \frac{\partial \vartheta}{\partial x_i} + \frac{\partial \sigma_{ij}}{\partial x_j} = 0, \quad \text{and} \quad (44b)$$

$$\frac{3 + \delta}{2} \frac{\partial \theta}{\partial t} + \frac{\partial v_i}{\partial x_i} + \frac{\partial q_i}{\partial x_i} = 0, \quad (44c)$$

and the linearized balance equation of dynamic temperature, stress, and total heat fluxes are specified as

$$\frac{3}{2} \frac{D\vartheta}{Dt} + \frac{\delta}{3 + \delta} \frac{\partial v_i}{\partial x_k} + \frac{2\delta}{(3 + \delta)(5 + \delta)} \frac{\partial q_k}{\partial x_k} = \mathcal{P}^{0,0}. \quad (45)$$

$$\sigma_{ij} = -2\mu \frac{\partial v_{(i}}{\partial x_{j)}} \quad \text{and} \quad q_k = -\lambda \frac{\partial \theta}{\partial x_k} - \frac{2\lambda}{5 + \delta} \frac{\partial \vartheta}{\partial x_k}, \quad (46)$$

where $\lambda = \frac{(5+\delta)^2}{25} \zeta_{11}$ is thermal conductivity of gases.

VI. LINEAR STABILITY ANALYSIS

In this section, we examine both temporal and spatial stability analyses of the two temperature models derived in Sec. II with different coefficients given in Secs. 2.3.2 and 2.3.3. Now we consider a one-dimensional process (in the x direction) without any external forces and assume a plane wave solution of the form

$$\Phi = \Phi_a \exp[i(\omega t - kx)] \quad (47)$$

for Eqs. (39) and (40), where $\Phi = \{\rho, v_x, \theta^{\text{tr}}, \theta^{\text{in}}\}^T$, Φ_a is a vector containing the complex amplitudes of the respective waves, and ω and k are the dimensionless frequency and the wave number, respectively. Substitution of the plane wave solution (47) into Eqs. (39) and (40) gives a system of algebraic

equations $A\Phi = 0$, where

$$A(\omega, k) = \begin{bmatrix} i\omega & -ik & 0 & 0 \\ -ik & \frac{4k^2\mu}{3} + i\omega & -ik & 0 \\ 0 & -ik & \frac{3\delta P_{\text{fl}}^0}{2(3+\delta)} + k^2\zeta_{11} + \frac{3}{2}i\omega & -\frac{3\delta P_{\text{fl}}^0}{2(3+\delta)} + k^2\zeta_{12} \\ 0 & 0 & -\frac{3\delta P_{\text{fl}}^0}{2(3+\delta)} + k^2\zeta_{21} & \frac{3\delta P_{\text{fl}}^0}{2(3+\delta)} + k^2\zeta_{22} + \frac{\delta}{2}i\omega \end{bmatrix}. \tag{48}$$

This matrix is for the model 3 coefficients; in the same way, we will be driving for the other model’s coefficients. The analogous dispersion relation found when the determinate of $A(\omega, k)$ is zero is the relation between ω and k for nontrivial solutions. For temporal stability, a disturbance is considered in space; consequently, the wave number k is assumed to be real while the frequency $\omega = \omega_r(k) + i\omega_i(k)$ can be complex. The phase velocity v_{ph} and damping α of the corresponding waves are given by

$$v_{\text{ph}} = \frac{\omega_r(k)}{k} \quad \text{and} \quad \alpha = \omega_i(k).$$

The stability of equations may be tested in two ways: temporal stability and spatial stability. Temporal stability requires damping, and thus $\omega_i(k) \geq 0$. If, however, $\omega_i(k) \leq 0$, then a little disturbance in space will blow up in time. If a disturbance in time at a given location is considered, then the frequency ω is real, while the wave number is complex, $k = k_r(\omega) + ik_i(\omega)$. Phase velocity v_{ph} and damping α of the corresponding waves are given by

$$v_{\text{ph}} = \frac{\omega}{k_r(\omega)}, \quad \text{and} \quad \alpha = -k_i(\omega).$$

For a wave traveling in positive x direction ($k_r > 0$), the damping must be negative, while for a wave traveling in negative x direction ($k_r < 0$), the damping must be positive ($k_i > 0$).

We check how stable it is against small changes in frequency ω . As we’ve seen, stability needs different signs of the real and imaginary parts of $k(\omega)$. So, if $k(\omega)$ is plotted in the complex plane with ω as the parameter, the curves should not touch the upper right or lower left quadrants. Figures 1–5 (up) illustrate the solutions for the six-moment system, and we can see that all modes are inside the requisite stability field, indicating that none of the solutions violate the stability condition. In Figs. 1–5 (up) we analyze the stability against a disturbance of a specific wavelength, denoted by the wave number k . The figures show the damping coefficient α is positive for all k , and it follows that the six-moment system is stable. The two-temperature model equations are stable for all frequencies, as well as they are stable for disturbances of any wavelength. We can additionally show that the two-temperature model is stable for other gases ($\text{N}_2, \text{O}_2, \text{H}_2, \text{CO}_2$) as well.

VII. SOUND WAVE PROPAGATION

Wave propagation phenomena provide a valuable means to assess the validity of nonequilibrium thermodynamics theories. In this section, we focus on the study of plane harmonic waves and aim to compare the theoretical predictions of the

dispersion relation with experimental data. To ensure a more manageable analysis, we restrict our investigation to the one-dimensional spatial problem. To investigate the propagation in the x direction of high-frequency sound waves having an angular frequency and complex wave number $k = k_r + ik_i$ we write the plane wave solution of the form equation (47) and obtain a dispersion relation which is already discussed in

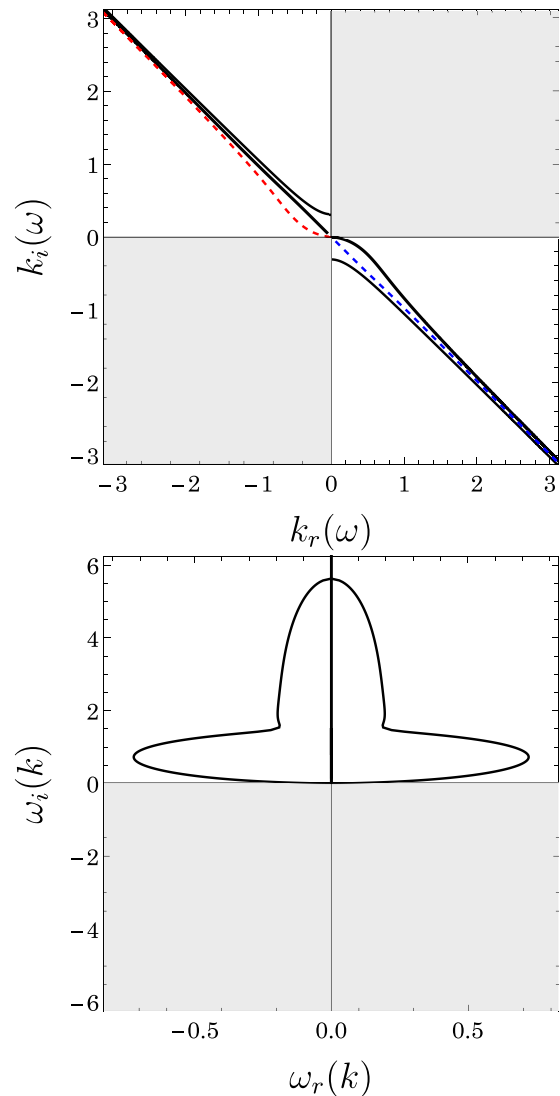


FIG. 1. Stability analysis of the two-temperature model for CH_4 gas with Model 1 coefficients: panel (up) spatial stability and panel (down) temporal stability. In panel (up) black, red, or blue dashed lines represent different modes corresponding to the parameter ω .

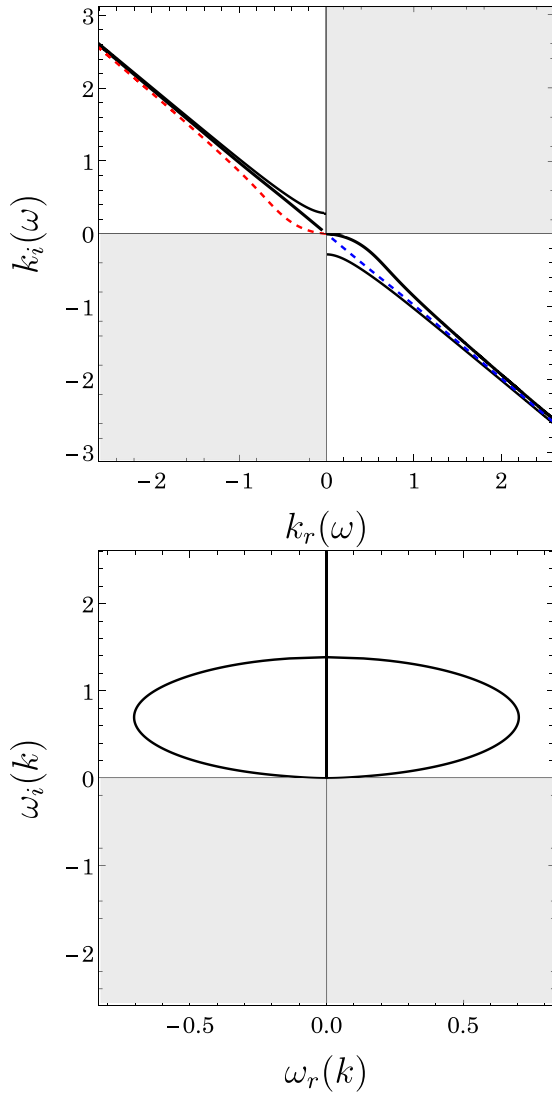


FIG. 2. Stability analysis of the two-temperature model for CH₄ gas with Model 2 coefficients: panel (up) spatial stability and panel (down) temporal stability. In panel (up) black, red, or blue dashed lines represent different modes corresponding to the parameter ω .

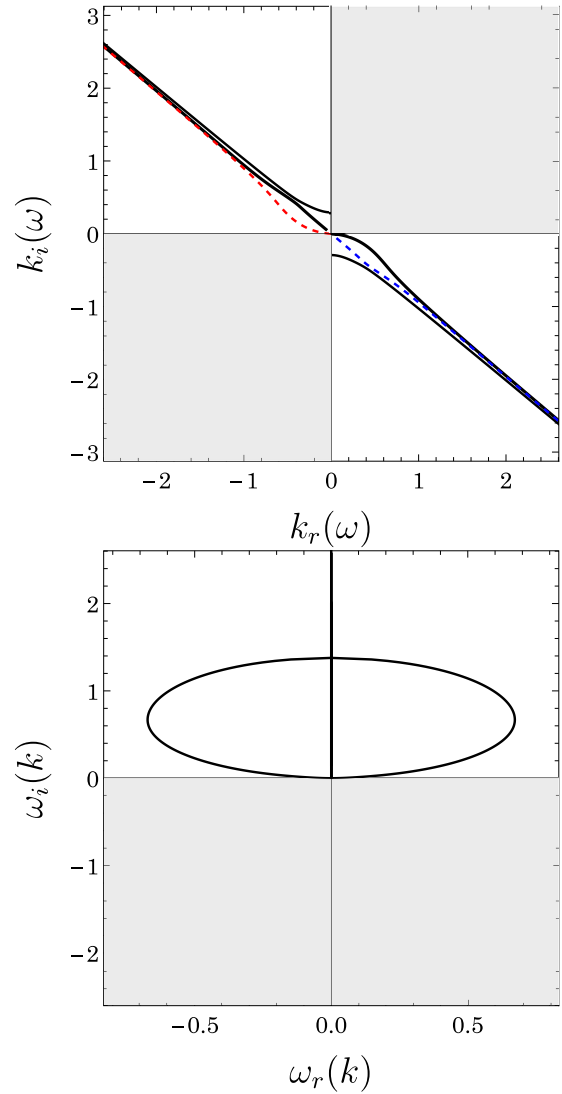


FIG. 3. Stability analysis of the two-temperature model for CH₄ gas with Model 3 coefficients: panel (up) spatial stability and panel (down) temporal stability. In panel (up) black, red, or blue dashed lines represent different modes corresponding to the parameter ω .

Sec. VI. The dispersion relation permits the calculation of the phase velocity v_{ph} and of the attenuation coefficient α in terms of the frequency ω :

$$v_{ph} = \frac{\omega}{k_r(\omega)}, \quad \text{and} \quad \alpha = -k_i(\omega).$$

A. Comparison with experimental data

The dispersion relation obtained from $\det(A) = 0$, in particular, the phase velocity v_{ph} , attenuation factor α and the speed of sound as the functions of the frequency ω are compared with the acoustic measurements of Greenspan in nitrogen (N₂) and oxygen (O₂) gases [28]. These sound propagation measurements were made at a temperature of 300 K in a 11 MHz double-crystal interferometer for different values of the gas pressure.

In Figs. 6–8 the attenuation factor $\alpha c_0/\omega$, the reciprocal speed ratio c_0/v_{ph} , and speed of sound $(v_{ph} - c_0)/c_0$ are shown on a double logarithmic scale as a function of the nonequilibrium parameter $p/\mu\omega$, which is the ratio of collision frequency in gas and frequency of the sound, for nitrogen and oxygen. The solid lines represent the theoretical sound propagation results derived from our theory and NSF (cyan line), while the red square box is the experimental data of Greenspan for sound waves. From the analysis of Figs. 6–8, it can be observed that in the low-frequency range ($p/\mu\omega \gg 1$), both our theories and the classical Navier-Stokes-Fourier (NSF) theory exhibit excellent agreement with experimental data for sound propagation. This agreement indicates that in near-equilibrium regime, our theory and the NSF theory yield comparable results. However, as the nonequilibrium parameter decreases and we move into a transition regime ($1 < p/\mu\omega < 10$), our theory shows improved

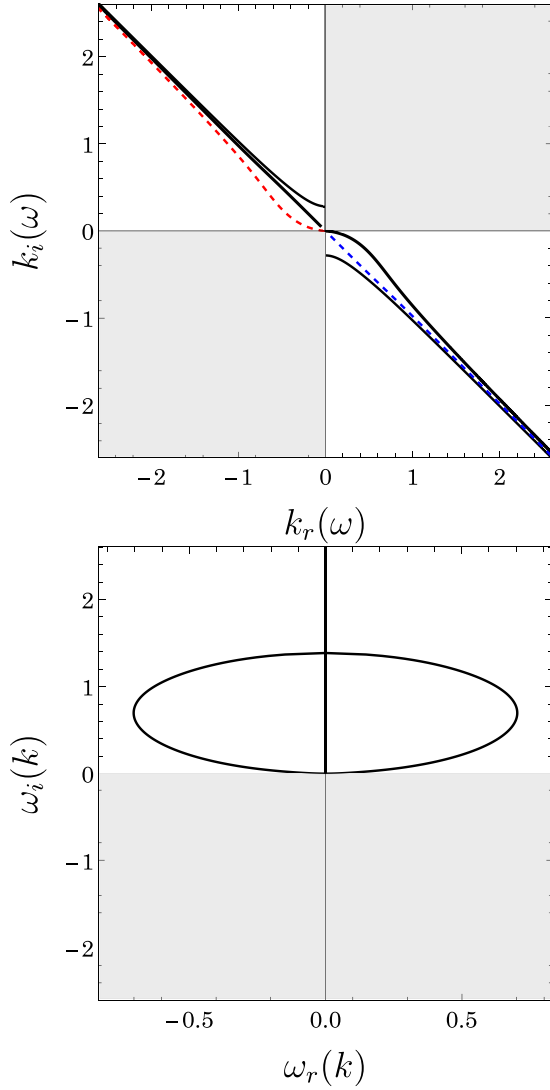


FIG. 4. Stability analysis of the two-temperature model for CH_4 gas with Model 4 coefficients: panel (up) spatial stability and panel (down) temporal stability. In panel (up) black, red, or blue dashed lines represent different modes corresponding to the parameter ω .

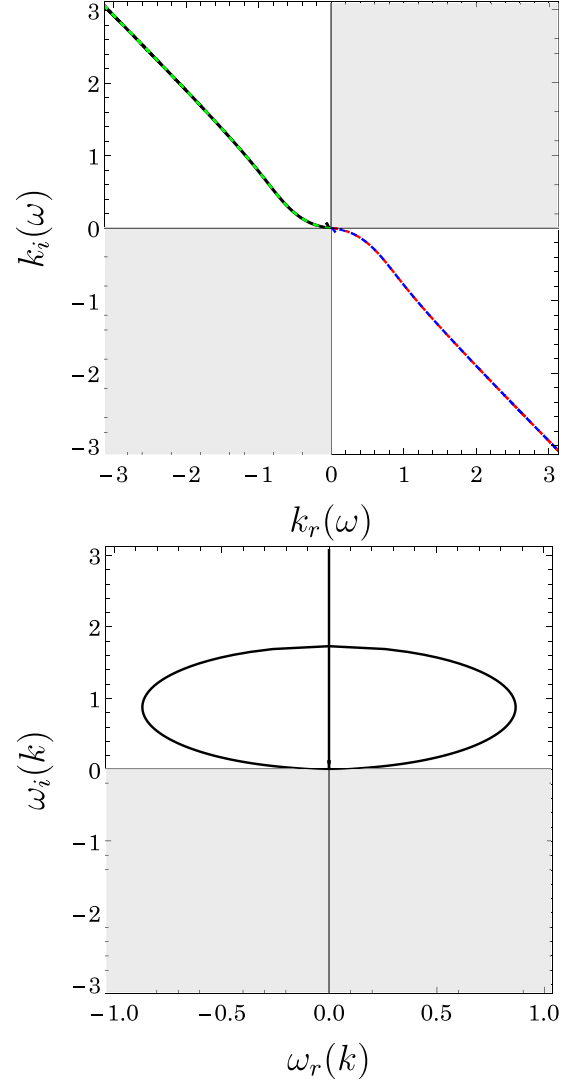


FIG. 5. Stability analysis of the two-temperature model for CH_4 gas with reduced model coefficients: panel (up) spatial stability and panel (down) temporal stability. In panel (up) black, red, green, or blue dashed lines represent different modes corresponding to the parameter ω .

performance compared to the classical NSF theory. Furthermore, in the high-frequency region ($p/\mu\omega < 1$), our theory consistently outperforms the classical NSF theory, as evident from Figs. 6–8.

VIII. SPONTANEOUS RAYLEIGH-BRILLOUIN SCATTERING

Spontaneous Rayleigh–Brillouin scattering (SRBs) in gases originates from instantaneous density fluctuation. A plane polarised light with the following parameters: intensity I_0 , angular frequency ω_0 , wave vector \mathbf{k}_0 , and polarization n_0 impacts a fluid with the following dielectric constant ϵ_0 . The light’s intensity, angular frequency ω_s , wave vector \mathbf{k}_s , and polarization n_s , which was detected at distance d from scattered volume a detector by the fluid’s scattering at angle θ

is given by

$$I(\mathbf{K}, \omega, d) = I_0 \frac{(\omega_0)^4}{16\pi^2 d^2 c^4} (n_0 \cdot n_s)^2 S(\mathbf{K}, \omega), \quad (49)$$

where c is the speed of light in a vacuum, $\omega = \omega_0 - \omega_s$ the shift in angular frequency and in a very close approximation, the wave vector \mathbf{K} of the fluctuation being observed is the momentum transfer between the incident wave vector \mathbf{k}_0 , the scattered wave vector \mathbf{k}_s and $S(\mathbf{K}, \omega)$ is dynamic structure factor. The magnitude of \mathbf{K} is then approximately equal to $|\mathbf{K}| = |\mathbf{k}_0 - \mathbf{k}_s| = 2|\mathbf{k}_0|\sin(\theta/2)$.

The hydrodynamic equations are straightforward due to the one-dimensional, linearized, and boundary conditions-free character, and thus enable analytical solutions for the Rayleigh-Brillouin-scattering problem [26,48]. The Knudsen number (Kn), which is defined as the ratio of the mean free

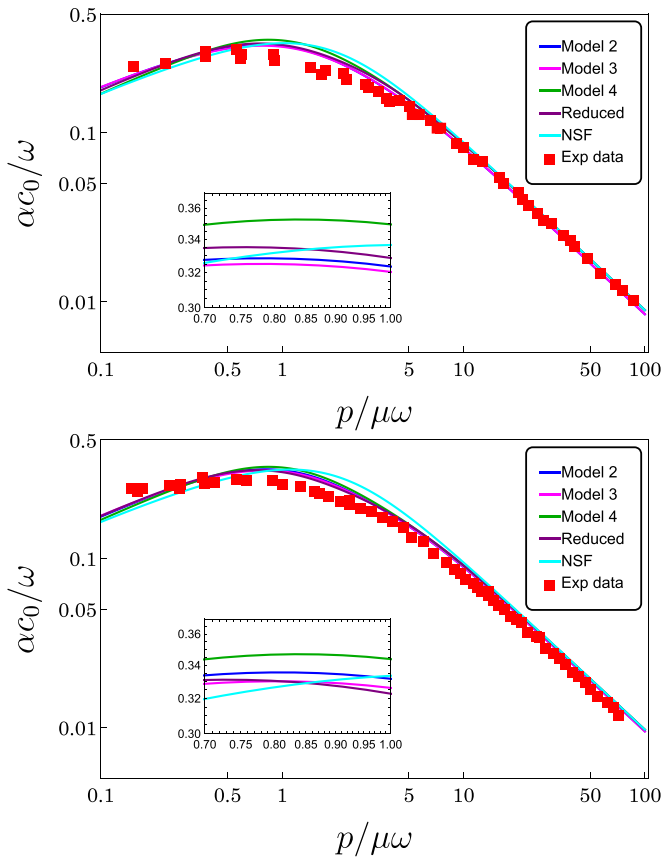


FIG. 6. Schematics for nitrogen (up) and oxygen (down), depicting the attenuation factor α_{c_0}/ω as a function of the rarefaction parameter $p/\mu\omega$ at a temperature of 300 K. The predictions of our theory using various coefficients and the Navier-Stokes-Fourier (NSF) theory are compared with experimental data obtained by Greenspan [28].

path of gas molecules to the characteristic length scale (L) of the system, known as the scattering wavelength $2\pi/\mathbf{K}$, is used to describe the spectrum of scattered light. The linearized and one-dimensional form of our system is

$$\frac{\partial \hat{\rho}}{\partial \hat{t}} + \frac{\partial \hat{v}}{\partial \hat{x}} = \delta(\hat{t}), \quad (50a)$$

$$\frac{\partial \hat{v}}{\partial \hat{t}} + \frac{\partial \hat{\rho}}{\partial \hat{x}} + \frac{\partial \hat{\theta}^{\text{tr}}}{\partial \hat{x}} + \frac{\partial \hat{\sigma}}{\partial \hat{x}} = 0, \quad (50b)$$

$$\frac{3}{2} \frac{\partial \hat{\theta}^{\text{tr}}}{\partial \hat{t}} + \frac{\partial \hat{v}}{\partial \hat{x}} + \frac{\partial \hat{q}^{\text{tr}}}{\partial \hat{x}} = \mathcal{P}^{0,0}, \quad (50c)$$

$$\frac{\delta}{2} \frac{\partial \hat{\theta}^{\text{in}}}{\partial \hat{t}} + \frac{\partial \hat{q}^{\text{in}}}{\partial \hat{x}} = \mathcal{P}^{0,1}, \quad (50d)$$

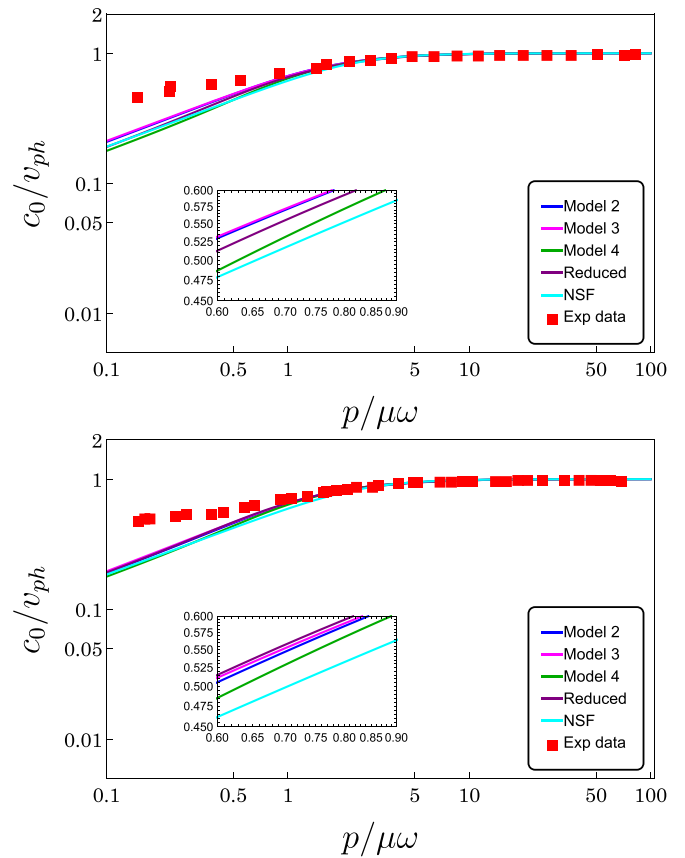


FIG. 7. Schematics for nitrogen (up) and oxygen (down), depicting the reciprocal speed ratio c_0/v_{ph} as a function of the rarefaction parameter $p/\mu\omega$ at a temperature of 300 K. The predictions of our theory using various coefficients and the Navier-Stokes-Fourier (NSF) theory are compared with experimental data obtained by Greenspan [28].

and constitutive equations

$$\hat{\sigma} = -\frac{4}{3} \text{Kn} \frac{\partial \hat{v}}{\partial \hat{x}}, \quad (51a)$$

$$\hat{q}^{\text{in}} = -\zeta_{12} \frac{\partial \hat{\theta}^{\text{tr}}}{\partial \hat{x}} - \zeta_{22} \frac{\partial \hat{\theta}^{\text{in}}}{\partial \hat{x}}, \quad \text{and} \quad (51b)$$

$$\hat{q}^{\text{tr}} = -\zeta_{11} \frac{\partial \hat{\theta}^{\text{tr}}}{\partial \hat{x}} - \zeta_{12} \frac{\partial \hat{\theta}^{\text{in}}}{\partial \hat{x}}. \quad (51c)$$

Equations (50) and (51) are transferred into the following matrix form by using the Laplace transform for the temporal variable t and the Fourier transform for the spatial variable x in the spontaneous SRB [26]:

$$\begin{bmatrix} -i\omega & 2\pi i & 0 & 0 \\ 2\pi i & -(i\omega - \frac{8\pi i}{3} \text{Kn}) & 2\pi i & 0 \\ 0 & 2\pi i & -\frac{3}{2}i\omega + 4\pi^2 \zeta_{11} & 4\pi^2 \zeta_{12} \\ 0 & 0 & 4\pi^2 \zeta_{12} & -\frac{\delta}{3}i\omega + 4\pi^2 \zeta_{22} \end{bmatrix} \begin{bmatrix} \hat{\rho} \\ \hat{v} \\ \hat{\theta}^{\text{tr}} \\ \hat{\theta}^{\text{in}} \end{bmatrix} = \begin{bmatrix} 1 \\ 0 \\ \mathcal{P}^{0,0} \\ \mathcal{P}^{0,1} \end{bmatrix}, \quad (52)$$

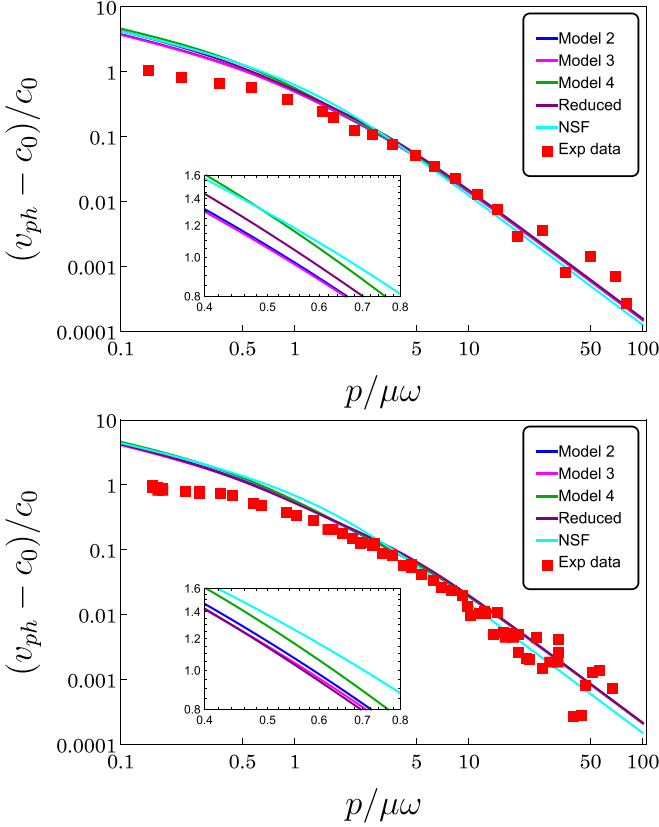


FIG. 8. Schematics for nitrogen (up) and oxygen (down), depicting speed of sound $(v_{ph} - c_0)/c_0$ as a function of the rarefaction parameter $p/\mu\omega$ at a temperature of 300 K. The predictions of our theory using various coefficients and the Navier-Stokes-Fourier (NSF) theory are compared with experimental data obtained by Greenspan [28].

where ω is the angular frequency. For the spectrum of the density fluctuations, $\hat{\rho}$, we solve the non-homogeneous matrix equations (52) and obtain the spontaneous Rayleigh–Brillouin scattering.

A. Results

In this section, analytic results for the light-scattering spectrum are derived for methane (CH_4) and compared with the predictions of the extended hydrodynamic theory of Hammond and Wiggins [49], which are entirely consistent with empirical data. To apply the two-temperature model to the results obtained in the previous section, certain conditions must be satisfied by the polyatomic gas. These conditions include spherical symmetry of the gas molecules and a specific heat capacity ratio close to $4/3$. Methane at ordinary temperatures approximately meets these requirements. By solving the non-homogeneous matrix equations (52) for the spectrum of the density fluctuations $\hat{\rho}$, we obtain the SRB spectra. An SRB spectrum typically consists of a central Rayleigh peak and two Brillouin side peaks at equidistant from the central Rayleigh peak. These Brillouin side peaks are located at $\sqrt{\frac{\gamma}{2}}$, where γ is the ratio of heat capacity. In the typical spectra of the SRBs,

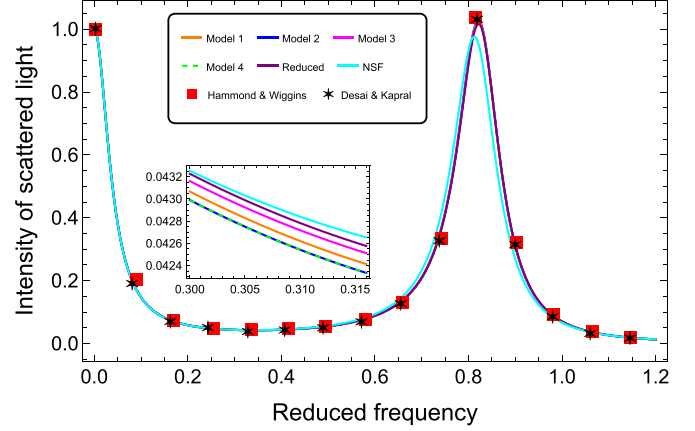


FIG. 9. The scattered light spectrum from CH_4 for $y = 18.27$ and spectrum has been normalized at the Rayleigh peak.

one can identify the contributions from the central Rayleigh peak and the Brillouin side peaks.

We show the scattered light spectrum from CH_4 gas (293 K and 1.013 bar) for different values of y , which is a measure of the ratio of the wavelength of the observed fluctuation with the collision mean free path

$$y = \frac{1}{\sqrt{2}} \left(\frac{k_b T_0}{m} \right)^{1/2} \frac{\rho_0}{\mu_0 \mathbf{K}}, \quad (53)$$

with the reduced frequency x is given by

$$x = \sqrt{\frac{2}{3}} \frac{\omega}{v_0 \mathbf{K}}, \quad (54)$$

here $v_0 = \sqrt{\frac{4}{3} RT_0}$ is the adiabatic speed of sound [26]. In Figs. 9–11, we compare the light-scattering results obtained from our two-temperature model equation with the predictions of the extended hydrodynamic theory proposed by Hammond and Wiggins [49]. The comparisons are made for three different values of parameter “ y ,” specifically 18.27, 4.46, and 2.70. Figures display the spectral predictions of the two-temperature model represented by solid and dashed lines, while the solid line (cyan color) represents the NSF model.

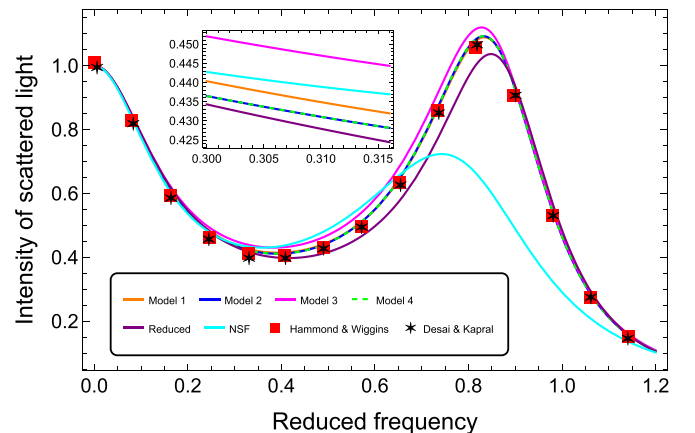


FIG. 10. The scattered light spectrum from CH_4 for $y = 4.46$ and spectrum has been normalized at the Rayleigh peak.

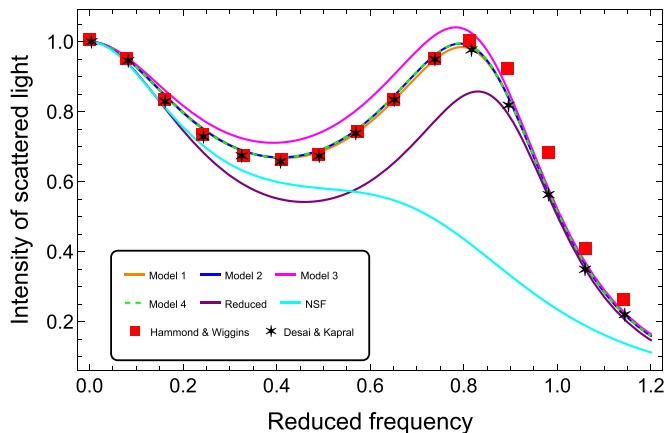


FIG. 11. The scattered light spectrum from CH_4 for $y = 2.70$ and spectrum has been normalized at the Rayleigh peak.

Additionally, the red square symbols represent the spectral prediction of the extended hydrodynamic theory, which, according to Hammond and Wiggins, exhibits excellent agreement with the experimental data (the curves are normalized at the zero frequency shift), and the diamond represents the prediction of the translational hydrodynamic theory from Desai and Kapral [50].

From Figs. 9–11, we can conclude that our two-temperature model accurately describes the Rayleigh-Brillouin spectrum in polyatomic ideal gases with rotational energy. Moreover, it demonstrates a smooth and precise transition between the hydrodynamic and kinetic regimes. This ability to provide a seamless connection between these two regimes enhances the model's capability to capture the behavior of the gas across a wide range of conditions.

Upon analyzing the results presented in Figs. 9–11, we observe that the reduced model provides favorable outcomes for $y = 18.27$ and $y = 4.46$ but exhibits slight discrepancies for $y = 2.70$. In contrast, the NSF approach fails to accurately predict the scattered light's spectrum from methane for $y = 4.46$ and $y = 2.70$. Based on these comparisons, we can conclude that the two-temperature model proposed in this work is well-suited for analyzing light-scattering experiments from methane.

It is important to note that the two-temperature model equation, as presented in this study, does not account for the vibrational degrees of freedom of the molecules, unlike the extended hydrodynamic model of Hammond and Wiggins [49]. Despite this limitation, the two-temperature model shows promise in providing valuable insights and predictions for light-scattering phenomena in polyatomic ideal gases with rotational energy, as demonstrated by its agreement with the extended hydrodynamic theory in certain cases.

Next, we have also compared the theoretical predictions of the two-temperature model with the molecular simulation method, specifically, molecular dynamics (MD), which completely agrees with direct simulation Monte Carlo [18]. This comparison allowed us to calculate the spontaneous Rayleigh-Brillouin-scattering spectra for gases such as N_2 and O_2 . These methods were achieved under an approximately fixed

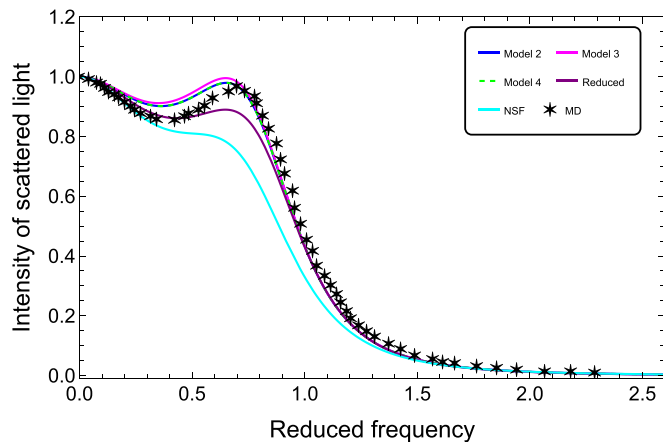


FIG. 12. The scattered light spectrum from N_2 for $y = 1.725$ and spectrum has been normalized at the Rayleigh peak.

pressure $P_0 = 3$ bar, temperature $T_0 \approx 298$ K, and wavelength of the laser is $L = 285$ nm. As thermodynamic parameters, we have utilized $\mu = 1.776 \times 10^{-5}$ Pa s and $\mu_b/\mu = 0.59$ for N_2 gas, as well as $\mu = 1.7825 \times 10^{-5}$ Pa s and $\mu_b/\mu = 0.54$ for O_2 gas, both at a temperature of $T_0 = 298$ K, as reported in Ref. [51]. Note that in this comparison, the frequency has been normalized using the values of 1.55012 GHz and 1.5509 GHz for N_2 gas and for O_2 gas, respectively.

In Figs. 12 and 13, we present a comparison of the spectra of spontaneous Rayleigh-Brillouin scattering (RBS) derived from both the two-temperature model and the Navier-Stokes-Fourier (NSF) theories with molecular dynamics. The theoretical predictions have been normalized to a value of 1 at $x = 0$. As depicted in Figs. 12 and 13, it is evident that the two-temperature model theory exhibits superior agreement with molecular dynamics when compared to the NSF theory.

IX. WALL BOUNDARY CONDITIONS

The incorporation of the second law of thermodynamics is critical in determining appropriate wall boundary conditions for gas dynamics models. It is imperative that the boundary

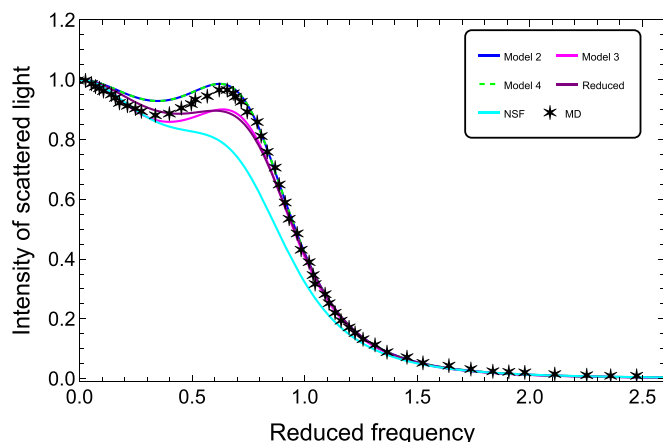


FIG. 13. The scattered light spectrum from O_2 for $y = 1.633$ and spectrum has been normalized at the Rayleigh peak.

conditions satisfy the second law to ensure that the entropy generation at the interface is positive.

Our approach to derive the boundary conditions is to evaluate the entropy generation at the interface and formulate the boundary conditions as phenomenological laws. The entropy generation can be computed using the entropy balance equation and integrating directly over the interface while applying Gauss's theorem.

The entropy production rate at the boundary Σ_w is given by the difference between the entropy fluxes into and out of the surface [12], i.e.,

$$\Sigma_w = \left(h_k - \frac{q_k^w}{\theta^w} \right) n_k. \quad (55)$$

Here, n_k is the unit normal pointing from the boundary into the gas, q_k^w denotes the heat flux in the wall at the interface, and θ^w denotes the temperature of the wall at the interface. Here, the wall is assumed to be a rigid Fourier heat conductor, with the entropy flux $\frac{q_k^w}{\theta^w}$.

At the interface, the total fluxes of mass, momentum, and energy are continuous, due to the conservation of these quantities,

$$v_k n_k = v_k^w n_k = 0, \quad (56a)$$

$$((p + \Pi)\delta_{ik} + \sigma_{ik})n_k = p^w n_i, \quad \text{and} \quad (56b)$$

$$((p + \Pi)v_k + \sigma_{ik}v_i + q_k)n_k = (p^w v_k^w + q_k^w)n_k, \quad (56c)$$

where all quantities with superscript w refer to wall properties, and the others refer to the gas properties. To proceed, we combine entropy generation and continuity conditions by eliminating the heat flux in the wall q_k^w and the pressure p^w , and find, after insertion of the entropy flux (26),

$$\Sigma_w = - \left[\frac{q_k}{\theta\theta^w} \mathcal{T} + \frac{2}{5 + \delta} \frac{\vartheta}{\theta(\theta + \vartheta)} q_k + \frac{3 + \delta}{5 + \delta} \frac{\vartheta}{\theta(\theta + \vartheta)} Q_k + \sigma_{ik} \frac{\mathcal{V}_i}{\theta^w} \right] n_k. \quad (57)$$

Here, $\mathcal{V}_i = v_i - v_i^w$ is the slip velocity, with $\mathcal{V}_i n_i = 0$, and $\mathcal{T} = \theta - \theta^w$ is the temperature jump. To write the entropy generation properly as the sum of products of forces and fluxes, it is necessary to decompose the stress tensor and heat flux into their components in the normal and tangential directions as [30]

$$q_k = q_n n_k + \bar{q}_k, \quad (58a)$$

$$Q_k = Q_n n_k + \bar{Q}_k, \quad \text{and} \quad (58b)$$

$$\sigma_{ik} = \sigma_{nn} \left(\frac{3}{2} n_i n_k - \frac{1}{2} \delta_{ik} \right) + \bar{\sigma}_{ni} n_k + \bar{\sigma}_{nk} n_i + \tilde{\sigma}_{ik}, \quad (58c)$$

where $q_n = q_i n_i$, $\sigma_{nn} = \sigma_{jl} n_j n_l$, and

$$\bar{q}_k = q_k - q_n n_k, \quad (59a)$$

$$\bar{Q}_k = Q_k - Q_n n_k, \quad (59b)$$

$$\bar{\sigma}_{ni} = \sigma_{il} n_l - \sigma_{nn} n_i, \quad \text{and} \quad (59c)$$

$$\tilde{\sigma}_{ik} = \sigma_{ik} - \sigma_{nn} \left(\frac{3}{2} n_i n_k - \frac{1}{2} \delta_{ik} \right) - \bar{\sigma}_{ni} n_k - \bar{\sigma}_{nk} n_i, \quad (59d)$$

such that $\bar{q}_l n_l = \bar{\sigma}_{nl} n_l = \tilde{\sigma}_{il} = \tilde{\sigma}_{ik} n_k = \tilde{\sigma}_{ik} n_i = 0$. Substituting Eqs. (58) and (59) into Eq. (57), the entropy generation

can be written as a sum of three contributions:

$$\Sigma_w = - \frac{\mathcal{T}}{\theta\theta^w} \left[q_n - \frac{2}{5 + \delta} \frac{\vartheta}{\theta + \vartheta} q_n - \frac{3 + \delta}{5 + \delta} \frac{\vartheta}{\theta + \vartheta} Q_n + \bar{\sigma}_{ni} \mathcal{V}_i \right] - \frac{1}{\theta\theta^w} \frac{\vartheta\theta}{\theta + \vartheta} \left(\frac{2}{5 + \delta} q_n + \frac{3 + \delta}{5 + \delta} Q_n \right) - \frac{\mathcal{V}_i}{\theta} \bar{\sigma}_{ni}. \quad (60)$$

For a positive entropy production, we find the phenomenological boundary conditions for the two-temperature model as

$$q_n - \frac{2}{5 + \delta} \frac{\vartheta}{\theta + \vartheta} q_n - \frac{3 + \delta}{5 + \delta} \frac{\vartheta}{\theta + \vartheta} Q_n + \bar{\sigma}_{ni} \mathcal{V}_i = -\eta_{11} \mathcal{T} - \eta_{12} \frac{\vartheta}{\theta + \vartheta} \theta, \quad (61a)$$

$$\frac{2}{5 + \delta} q_n + \frac{3 + \delta}{5 + \delta} Q_n = -\eta_{12} \mathcal{T} - \eta_{22} \frac{\vartheta}{\theta + \vartheta} \theta, \quad (61b)$$

$$\bar{\sigma}_{ni} = -\Xi \mathcal{V}_i. \quad (61c)$$

Here, the matrices

$$\eta = \begin{bmatrix} \eta_{11} & \eta_{12} \\ \eta_{12} & \eta_{22} \end{bmatrix} \quad (62)$$

is a symmetric nonnegative definite matrix of Onsager resistivity coefficients and $\Xi \geq 0$, which can be obtained either from experiments or from kinetic theory models, as we shall show in next sections.

A. Comparison with Rahimi and Struchtrup [19]

The Onsager resistivity coefficients (η_{ij}) appearing in the boundary conditions Eqs. (61) are obtained from kinetic theory in the asymptotic limit of small dynamic temperature ($\vartheta \rightarrow 0$):

$$\eta_{11} = \frac{\chi}{2 - \chi} \frac{(4 + \delta)}{2} p \sqrt{\frac{2}{\pi\theta}} + O(\min(\epsilon^\alpha, \epsilon)), \quad (63a)$$

$$\eta_{12} = \frac{1}{2} \frac{\chi}{2 - \chi} p \sqrt{\frac{2}{\pi\theta}} + O(\min(\epsilon^\alpha, \epsilon)), \quad (63b)$$

$$\eta_{22} = \frac{\chi}{2 - \chi} \sqrt{\frac{2}{\pi\theta}} p \left[\frac{15 + 4\delta(3 + \delta)}{2\delta(5 + \delta)} + \frac{1}{(3 + \delta)} \right] + O(\min(\epsilon^\alpha, \epsilon)), \quad (63c)$$

$$\Xi = \frac{\chi}{2 - \chi} \sqrt{\frac{2}{\pi\theta}} p + O(\min(\epsilon^\alpha, \epsilon)), \quad (63d)$$

where χ is the wall accommodation coefficients, specifying the level of accommodation of the particle on the wall. Full accommodation is specified by $\chi = 1$ and the pure specularly reflected particles are described by $\chi = 0$. Solving boundary conditions Eqs. (61) for q_n and Q_n and after that linearized and we obtain

$$q_n = -\eta_{11} \mathcal{T} - \eta_{12} \vartheta, \quad (64)$$

$$Q_n = -\frac{5 + \delta}{3 + \delta} \left[\eta_{12} - \frac{2}{5 + \delta} \eta_{11} \right] \mathcal{T} - \frac{5 + \delta}{3 + \delta} \left[\eta_{22} - \frac{2}{5 + \delta} \eta_{12} \right] \vartheta. \quad (65)$$

Now substitute the value of coefficients from Eq. (63) in phenomenological boundary conditions (61) and linearized, dimensionless, we get the following boundary conditions:

$$\hat{q}_n = -\frac{\chi}{2-\chi} \sqrt{\frac{2}{\pi}} \frac{(4+\delta)}{2} \hat{\mathcal{F}} - \frac{\chi}{2-\chi} \sqrt{\frac{2}{\pi}} \frac{1}{2} \hat{\vartheta}, \quad (66a)$$

$$\hat{Q}_n = \frac{1}{2} \frac{\chi}{2-\chi} \sqrt{\frac{2}{\pi}} \hat{\mathcal{F}} - \frac{\chi}{2-\chi} \sqrt{\frac{2}{\pi}} \left[\frac{15+4\delta}{2\delta} + \frac{2}{(3+\delta)^2} \right] \hat{\vartheta}, \quad (66b)$$

$$\hat{\sigma}_{ni} = -\frac{\chi}{2-\chi} \sqrt{\frac{2}{\pi}} \hat{\mathcal{V}}_i. \quad (66c)$$

B. Reduced model boundary condition

For Reduced model boundary condition $Q_n = 0$, i.e.,

$$\eta_{12} = \frac{2}{5+\delta} \eta_{11} \quad \text{and} \quad \eta_{22} = \frac{4}{(5+\delta)^2} \eta_{11}. \quad (67)$$

Upon substituting the values of these coefficients from Eq. (67) into the phenomenological boundary conditions (61), and linearizing and dimensionless the equations, we obtain the following boundary conditions:

$$\hat{q}_n = -\frac{\chi}{2-\chi} \sqrt{\frac{2}{\pi}} \frac{4+\delta}{2} \hat{\mathcal{F}} - \frac{\chi}{2-\chi} \sqrt{\frac{2}{\pi}} \frac{4+\delta}{5+\delta} \hat{\vartheta}, \quad (68a)$$

$$\hat{\sigma}_{ni} = -\frac{\chi}{2-\chi} \sqrt{\frac{2}{\pi}} \hat{\mathcal{V}}_i. \quad (68b)$$

Furthermore, we compare the boundary conditions (64) and (61c) derived in the reduced model with those established by Jun Zhang *et al.* in their work [52]. Their study focused on slip velocity and temperature jump in single-species gases, utilizing the Cercignani-Lampis-Lord model. In this model, the slip velocity depends only on the tangential accommodation coefficient, while the temperature jump is affected by accommodation coefficients in both the tangential and normal directions. After comparison, obtain the following coefficients:

$$\eta_{11} = \frac{5(\alpha_p + \alpha_t)}{2(10 - 3\alpha_{p-2\alpha_t})} \sqrt{\frac{8}{\pi}} \quad \text{and} \quad \Xi = \frac{\beta_t}{2 - \beta_t} \sqrt{\frac{2}{\pi}}, \quad (69)$$

where α_t and α_p represent the two accommodation coefficients for tangential and normal energy, respectively. Additionally, there is the tangential momentum accommodation coefficient β_t , which is related to α_t through the equation $\alpha_t = \beta_t(2 - \beta_t)$.

X. HEAT TRANSFER BETWEEN TWO PARALLEL PLATES

This section focuses on the validation of our wall boundary conditions through an investigation of a fundamental problem involving steady-state conductive heat transfer through stationary rarefied gases confined between parallel plates. To achieve this, we employ the two-temperature model within the framework of rarefied gas dynamics.

A. Problem settings and reduced moment equations

In this study, we investigate a steady-state gas flow between two parallel plates that are infinitely long and fixed perpendicular to the y axis at $y = \pm 1/2$ (see Fig. 14). The temperature of the walls differs, and the flow properties and variables solely depend on the y direction. The fluid is assumed to be stationary in this case, and any flow caused by density changes in an unsteady state is ignored. The two temperature model equation (39) can be derived for one-dimensional channel flows by omitting partial derivatives with respect to x and z . Thus, the conservation laws are modified in this form

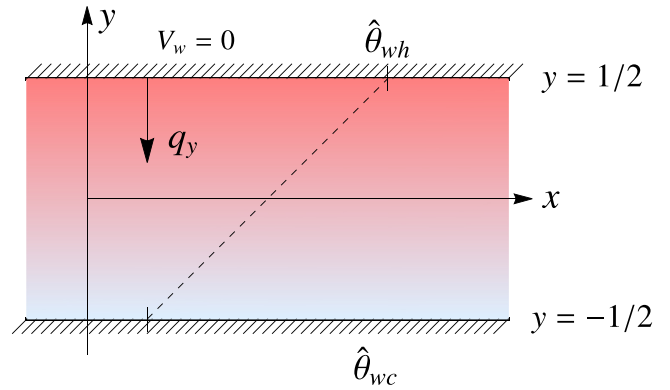


FIG. 14. The schematic illustrates heat conduction, featuring a channel with two stationary parallel walls having distinct temperatures.

ular to the y axis at $y = \pm 1/2$ (see Fig. 14). The temperature of the walls differs, and the flow properties and variables solely depend on the y direction. The fluid is assumed to be stationary in this case, and any flow caused by density changes in an unsteady state is ignored. The two temperature model equation (39) can be derived for one-dimensional channel flows by omitting partial derivatives with respect to x and z . Thus, the conservation laws are modified in this form

$$\begin{aligned} \frac{\partial \hat{\sigma}_{xy}}{\partial \hat{y}} &= 0, & \frac{\partial \hat{\rho}}{\partial \hat{y}} + \frac{\partial \hat{\theta}}{\partial \hat{y}} + \frac{\partial \hat{\vartheta}}{\partial \hat{y}} + \frac{\partial \hat{\sigma}_{yy}}{\partial \hat{y}} &= 0, \\ \text{and} \quad \frac{\partial \hat{q}_y}{\partial \hat{y}} &= 0, \end{aligned} \quad (70)$$

and equations of dynamic temperature

$$\left(\frac{2\delta}{(3+\delta)(5+\delta)} \right) \frac{\partial \hat{q}_y}{\partial \hat{y}} + \left(\frac{\delta}{5+\delta} \right) \frac{\partial \hat{Q}_y}{\partial \hat{y}} = \mathcal{P}^{0,0}. \quad (71)$$

The equation of stress tensor $\hat{\sigma}_{xy}$, total heat flux \hat{q}_y and heat difference \hat{Q}_y are

$$\hat{\sigma}_{xy} = -\frac{4Kn}{3} \frac{\partial \hat{\vartheta}}{\partial \hat{y}}, \quad (72a)$$

$$\begin{aligned} \hat{q}_y &= -(\zeta_{11} + 2\zeta_{12} + \zeta_{22}) \frac{\partial \hat{\theta}}{\partial \hat{y}} \\ &\quad - \left[(\zeta_{11} + \zeta_{12}) - \frac{3}{\delta} (\zeta_{12} + \zeta_{22}) \right] \frac{\partial \hat{\vartheta}}{\partial \hat{y}}, \end{aligned} \quad (72b)$$

$$\begin{aligned} \hat{Q}_y &= - \left[\left(\zeta_{11} - \frac{5}{\delta} \zeta_{12} \right) + \left(\zeta_{12} - \frac{5}{\delta} \zeta_{22} \right) \right] \frac{\partial \hat{\theta}}{\partial \hat{y}} \\ &\quad - \left[\left(\zeta_{11} - \frac{5}{\delta} \zeta_{12} \right) - \frac{3}{\delta} \left(\zeta_{12} - \frac{5}{\delta} \zeta_{22} \right) \right] \frac{\partial \hat{\vartheta}}{\partial \hat{y}}. \end{aligned} \quad (72c)$$

The linear system can be easily solved analytically, yielding the general solution that involves seven constants to be determined. One of the constants depends on the average density between the plates: upon setting the range of y to be $[-1/2, 1/2]$ (so that $L = 1$), we assign the average density as

$$\int_{-1/2}^{1/2} \hat{\rho}(y) dy = 0. \quad (73)$$

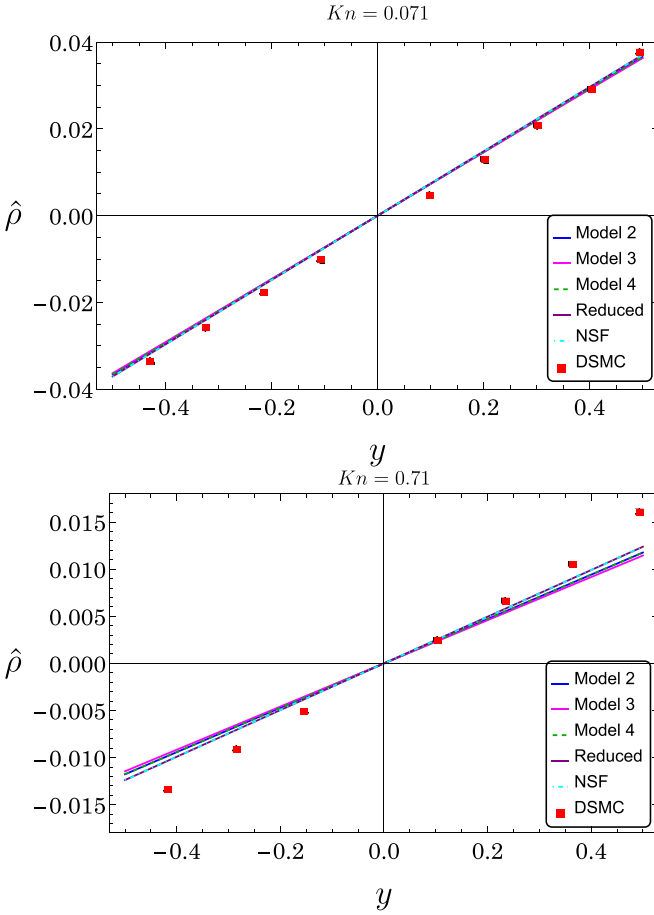


FIG. 15. Comparison of density profiles for Kn numbers equal to 0.071 (up) and 0.71 (down). Results shown are obtained from: our theory (solid, dashed line); NSF equations (dot dashed cyan line); DSMC method (red square box) [53].

The remaining six constants can be determined through six boundary conditions. In the one-dimensional setting, each boundary contributes three boundary conditions, as specified by Eq. (66). Here, we present the boundary conditions specifically for the upper wall:

$$\hat{q}_y = -\frac{\chi}{2-\chi} \sqrt{\frac{2}{\pi}} \frac{(4+\delta)}{2} \hat{\mathcal{T}} - \frac{\chi}{2-\chi} \sqrt{\frac{2}{\pi}} \frac{1}{2} \hat{\mathcal{T}}, \quad (74a)$$

$$\hat{Q}_y = \frac{1}{2} \frac{\chi}{2-\chi} \sqrt{\frac{2}{\pi}} \hat{\mathcal{T}} - \frac{\chi}{2-\chi} \sqrt{\frac{2}{\pi}} \left[\frac{15+4\delta}{2\delta} + \frac{2}{(3+\delta)^2} \right] \hat{\mathcal{T}}, \quad (74b)$$

$$\hat{\sigma}_{xy} = -\frac{\chi}{2-\chi} \sqrt{\frac{2}{\pi}} \hat{\mathcal{V}}_2. \quad (74c)$$

To apply the boundary conditions on the lower solid wall, it is sufficient to make the following parameter replacement:

$$\hat{q}_y \rightarrow -\hat{q}_y, \quad \hat{Q}_y \rightarrow -\hat{Q}_y, \quad \hat{\sigma}_{xy} \rightarrow -\hat{\sigma}_{xy}. \quad (75)$$

B. Results

We compare the results of two-temperature model with the Direct Simulation Monte Carlo (DSMC) method data [53]. Comparison between the analytical solution of

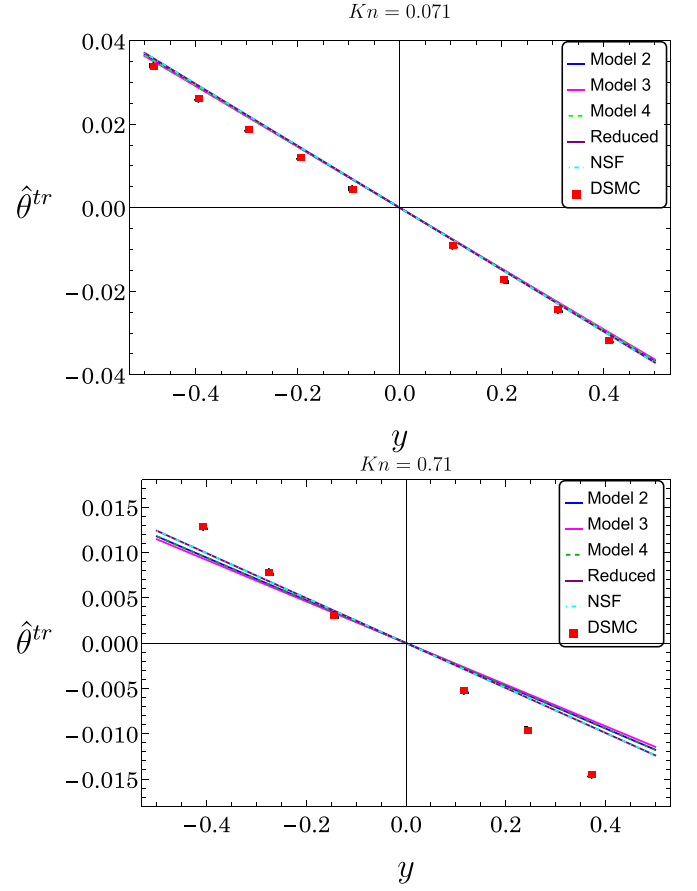


FIG. 16. Comparison of translational temperature for Kn numbers equal to 0.071 (up) and 0.71 (down). Results shown are obtained from: our theory (solid, dashed line); NSF equations (dot dashed cyan line); DSMC method (red square box) [53].

two-temperature model and DSMC results are shown in Figs. 15–17. Dimensionless wall temperatures are at deviations of ± 0.0476 from reference temperature at 350 K. We investigate two different reference Kn numbers, 0.071 and 0.71, which represent slip and transition flow regimes, respectively. Also, excited internal degrees of freedom is set to 2, the same as the DSMC simulation. Figures 15–17 clearly demonstrates the strong agreement between the DSMC and two-temperature model results in slip flow regimes. Furthermore, in the transition regime, two-temperature model exhibits even better agreement compared to the classical NSF theory. For Kn = 0.071 and Kn = 0.71, we determine the total heat flux (\hat{q}_y) to be approximately 0.025 and 0.084, respectively. As can be seen, the agreement between the curves of the two-temperature model solutions and the data from the DSMC reference solutions is evident, especially for smaller Knudsen numbers (Kn), indicating the accuracy and validity of two-temperature model and boundary conditions.

XI. CONCLUSIONS

By integrating concepts from various approaches to irreversible thermodynamics, including LIT, RT, and RET, we have developed an enhanced set of constitutive relations for

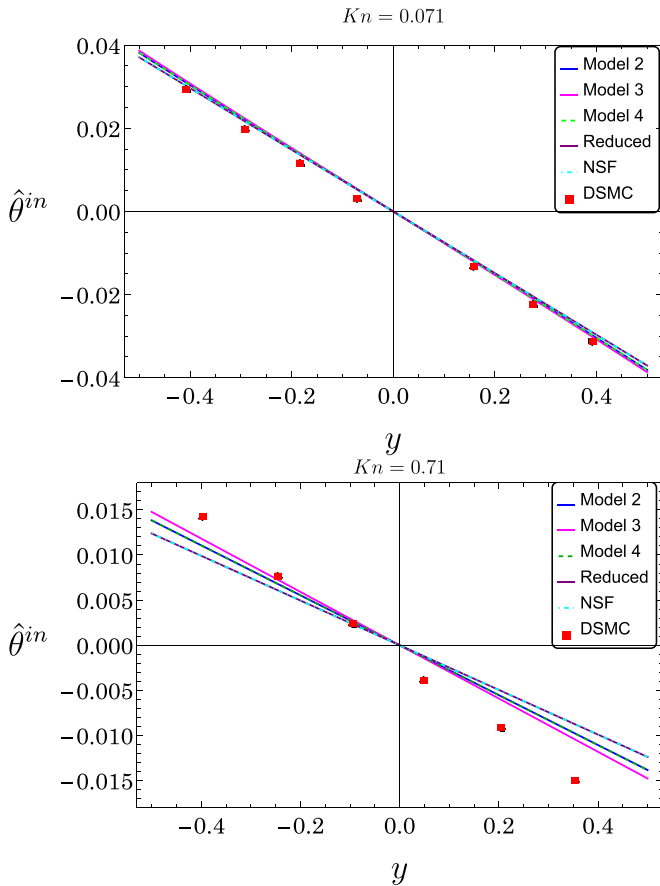


FIG. 17. Comparison of internal temperature for Kn numbers equal to 0.071 (up) and 0.71 (down). Results shown are obtained from: our theory (solid, dashed line); NSF equations (dot dashed cyan line); DSMC method (red square box) [53].

the stress tensor and heat flux within the framework of the two-temperature model. The two-temperature model has been provided with boundary conditions that ensure thermodynamic consistency. These conditions include descriptions of velocity slip, temperature jump, and transpiration flow at the boundaries.

In this paper, a two-temperature model equation has been applied to the analysis of sound propagation, light-scattering experiments, and heat transfer between two parallel plates in dilute polyatomic gases at room temperatures.

The comparison of our analytical solutions with acoustic and laser-scattering experiments conducted in nitrogen, oxygen, carbon dioxide, and methane at room temperatures demonstrates the excellent performance of the two-temperature model equation proposed in this study. The model proves to be highly effective in accurately describing time-dependent phenomena in polyatomic gases, yielding satisfactory agreement with experimental observations. We also solved steady one-dimensional stationary heat conduction analytically with a set of six-moment equations and compared the results with DSMC simulations.

In this paper, we have established the linear stability of the equations governing the two-temperature model for disturbances across all wavelengths or frequencies.

In subsequent research endeavors, there is potential for the development of second law preserving numerical techniques [54] tailored for nonlinear flows. Additionally, alternative numerical approaches like the method of fundamental solutions [55,56] warrant investigation. Furthermore, the expansion of the two-temperature model to encompass more comprehensive hydrodynamic models, including CCR polyatomic [57] and extended moments models [19], is part of the forthcoming agenda.

ACKNOWLEDGMENTS

A.K. gratefully acknowledges the financial support from the Council of Scientific and Industrial Research (CSIR) [File No. 09/719(0120)/2020-EMR-I]. A.S.R. acknowledges the financial support from the Science and Engineering Research Board, India, through Grants No. SRG/2021/000790 and No. MTR/2021/000417.

APPENDIX

The maximum entropy distribution function which maximizes the entropy (19) under the constraints (3), (5), and (6) takes the following form:

$$f_6 = \frac{\rho}{m} \underbrace{\frac{1}{\sqrt{2\pi}\theta_{tr}^3} e^{-\frac{c^2}{2\theta_{tr}}}}_{\text{Maxwellian}} \underbrace{\frac{1}{\gamma(\frac{\delta}{2})} \frac{1}{I} \left(\frac{I}{\theta^{in}}\right)^{\delta/2}}_{\text{Gamma}} e^{-\frac{I}{\theta^{in}}}.$$

Proof. The proof of the theorem employs the Lagrange multiplier method. To achieve this, we introduce a vector of multipliers $(\xi_0, \xi_i, \xi_1, \xi_2)$ and define the corresponding functional:

$$\begin{aligned} \mathcal{L}[f] = & -k_b \int f \ln \frac{f}{f_0} dCdI + \xi_0 \left\{ \rho - m \int f dCdI \right\} \\ & - \xi_i m \int f C_i dCdI + \xi_1 \left\{ \frac{3}{2} \rho \theta^{tr} - m \int f \frac{C^2}{2} dCdI \right\} \\ & + \xi_2 \left\{ \frac{\delta}{2} \rho \theta^{in} - m \int f I dCdI \right\}. \end{aligned} \tag{A1}$$

Taking the derivative of the functional \mathcal{L} with respect to f and setting it to zero

$$\frac{\partial \mathcal{L}}{\partial f} = -k_b \left(1 + \ln \frac{f}{f_0} \right) - \xi_0 m - \xi_i m C_i - m \xi_1 \frac{C^2}{2} - m \xi_2 I = 0.$$

Therefore, the solution of the Euler-Lagrange equation $\frac{\partial \mathcal{L}}{\partial f} = 0$ is given by

$$f_6 = f_0 \exp \left(-1 - \frac{\xi_0}{R} - \frac{\xi_i}{R} C_i - \frac{\xi_1}{R} \frac{C^2}{2} - \frac{\xi_2}{R} I \right). \tag{A3}$$

Put the value of f_6 in the constraint (3)

$$\rho = m \int e^{-1 - \frac{\xi_0}{R} - \frac{\xi_i}{R} C_i - \frac{\xi_1}{R} \frac{C^2}{2} - \frac{\xi_2}{R} I} dCdI, \tag{A4}$$

$$\rho = m e^{-(1 + \frac{\xi_0}{R})} A^{-(\delta/2)} \gamma(\delta/2) \frac{2\sqrt{2\pi}^{\frac{3}{2}}}{B^{\frac{3}{2}}}, \tag{A5}$$

where $\delta > 0$, $B = \frac{\xi_1}{R} > 0$, and $A = \frac{\xi_2}{R} > 0$.

Put the value of f_6 in the constraint (5)

$$\frac{3}{2}\rho\theta^{\text{tr}} = m \int e^{-1-\frac{\xi_0}{R}} I^{(\delta/2-1)} e^{-\frac{\xi_1}{R} \frac{c^2}{2}} e^{-\frac{\xi_2}{R} I} \frac{C^2}{2} dC dI, \quad (\text{A6})$$

$$\frac{3}{2}\rho\theta^{\text{tr}} = m e^{-1-\frac{\xi_0}{R}} \frac{3\sqrt{2\pi}^{\frac{3}{2}}}{B^{\frac{5}{2}}} A^{-(\delta/2)} \gamma(\delta/2). \quad (\text{A7})$$

Put the value of f_6 in the constraint (6),

$$\frac{\delta}{2}\rho\theta^{\text{in}} = m \int e^{-1-\frac{\xi_0}{R}} I^{(\delta/2)} e^{-\frac{\xi_1}{R} \frac{c^2}{2}} e^{-\frac{\xi_2}{R} I} dC dI, \quad (\text{A8})$$

$$\frac{\delta}{2}\rho\theta^{\text{in}} = m e^{-1-\frac{\xi_0}{R}} \frac{2\sqrt{2\pi}^{\frac{3}{2}}}{B^{\frac{3}{2}}} A^{-(1+\frac{\delta}{2})} \gamma\left(1 + \frac{\delta}{2}\right). \quad (\text{A9})$$

Solving Eqs. (A5), (A7), and (A9) we find the value of Lagrange multiplier as follows:

$$e^{-1-\frac{\xi_0}{R}} = \frac{\rho}{m} \frac{1}{\sqrt{2\pi\theta^{\text{tr}}{}^3}} \left[\frac{1}{\theta^{\text{in}}} \right]^{\frac{\delta}{2}} \frac{1}{\gamma(\delta/2)}, \quad (\text{A10})$$

$$\xi_1 = \frac{R}{\theta^{\text{tr}}}, \quad \xi_i = 0, \quad \text{and} \quad \xi_2 = \frac{R}{\theta^{\text{in}}}. \quad (\text{A11})$$

Substitute these values in Eq. (A3), and we find the following maximum entropy distribution function

$$f_6 = \frac{\rho}{m} \frac{1}{\sqrt{2\pi\theta^{\text{tr}}{}^3}} e^{-\frac{c^2}{2\theta^{\text{tr}}}} \frac{1}{\gamma(\frac{\delta}{2})} \frac{1}{I} \left[\frac{I}{\theta^{\text{in}}} \right]^{\frac{\delta}{2}} e^{-\frac{I}{\theta^{\text{in}}}}. \quad (\text{A12})$$

- [1] J. W. Strutt, On the light from the sky, its polarization and colour, *Philos. Mag. J. Sci.* **41**, 107 (1871).
- [2] V. Kara, V. Yakhot, and K. L. Ekinici, Generalized Knudsen number for unsteady fluid flow, *Phys. Rev. Lett.* **118**, 074505 (2017).
- [3] B. Sharma, R. Kumar, P. Gupta, S. Pareek, and A. Singh, On the estimation of bulk viscosity of dilute nitrogen gas using equilibrium molecular dynamics approach, *Phys. Fluids* **34**, 057104 (2022).
- [4] B. Sharma and R. Kumar, Estimation of bulk viscosity of dilute gases using a nonequilibrium molecular dynamics approach, *Phys. Rev. E* **100**, 013309 (2019).
- [5] E. Kustova, M. Mekhonoshina, A. Bechina, S. Lagutin, and Y. Voroshilova, Continuum models for bulk viscosity and relaxation in polyatomic gases, *Fluids* **8**, 48 (2023).
- [6] K. Aoki, M. Bisi, M. Groppi, and S. Kosuge, A note on the steady Navier–Stokes equations derived from an ES–BGK model for a polyatomic gas, *Fluids* **6**, 32 (2021).
- [7] T. Ruggeri and M. Sugiyama, *Rational Extended Thermodynamics beyond the Monatomic Gas* (Springer, Berlin, 2015).
- [8] E. Kustova and M. Mekhonoshina, Multi-temperature vibrational energy relaxation rates in CO₂, *Phys. Fluids* **32**, 096101 (2020).
- [9] K. Aoki, M. Bisi, M. Groppi, and S. Kosuge, Two-temperature Navier–Stokes equations for a polyatomic gas derived from kinetic theory, *Phys. Rev. E* **102**, 023104 (2020).
- [10] M. Bisi and G. Spiga, A two-temperature six-moment approach to the shock wave problem in a polyatomic gas, *Ricerche di Matematica* **68**, 1 (2019).
- [11] W. Dreyer, Maximisation of the entropy in nonequilibrium, *J. Phys. A: Math. Gen.* **20**, 6505 (1987).
- [12] S. R. De Groot and P. Mazur, *Non-equilibrium Thermodynamics* (Courier Corporation, Boston, MA, 2013).
- [13] B. D. Coleman and W. Noll, The thermodynamics of elastic materials with heat conduction and viscosity, *Arch. Rational Mech. Anal.* **13**, 167 (1963).
- [14] I. Müller and T. Ruggeri, *Rational Extended Thermodynamics* (Springer Science & Business Media, Cham, 2013), Vol. 37.
- [15] I. Müller, *Thermodynamics* (Pitman, Boston, MA, 1985).
- [16] S. Chapman and T. G. Cowling, *The Mathematical Theory of Nonuniform Gases: An Account of the Kinetic Theory of Viscosity, Thermal Conduction, and Diffusion in Gases* (Cambridge University Press, Cambridge, UK, 1990).
- [17] C. Cercignani, *Rarefied Gas Dynamics: From Basic Concepts to Actual Calculations* (Cambridge University Press, Cambridge, UK, 2000), Vol. 21.
- [18] Q. Ma, C. Yang, D. Bruno, and J. Zhang, Molecular simulation of Rayleigh–Brillouin scattering in binary gas mixtures and extraction of the rotational relaxation numbers, *Phys. Rev. E* **104**, 035109 (2021).
- [19] B. Rahimi and H. Struchtrup, Macroscopic and kinetic modelling of rarefied polyatomic gases, *J. Fluid Mech.* **806**, 437 (2016).
- [20] V. A. Rykov, A model kinetic equation for a gas with rotational degrees of freedom, *Fluid Dyn.* **10**, 959 (1976).
- [21] E. M. Shakhov, Generalization of the Krook kinetic relaxation equation, *Fluid Dyn.* **3**, 95 (1972).
- [22] H. Struchtrup and M. Torrilhon, Regularized 13 moment equations for hard sphere molecules: Linear bulk equations, *Phys. Fluids* **25**, 052001 (2013).
- [23] H. Struchtrup, Stable transport equations for rarefied gases at high orders in the Knudsen number, *Phys. Fluids* **16**, 3921 (2004).
- [24] P. Andries, P. Le Tallec, J.-P. Perlat, and B. Perthame, The Gaussian-BGK model of Boltzmann equation with small Prandtl number, *Eur. J. Mech. B Fluids* **19**, 813 (2000).
- [25] V. Djordjić, G. Oblapenko, M. Pavić-Čolić, and M. Torrilhon, Boltzmann collision operator for polyatomic gases in agreement with experimental data and DSMC method, *Continuum Mech. Thermodyn.* **35**, 103 (2023).
- [26] W. Marques Jr. and G. M. Kremer, Spectral distribution of scattered light in polyatomic gases, *Physica A* **197**, 352 (1993).
- [27] G. M. Kremer, Kinetic theory of a rarefied gas of rough spheres, *Revista Brasileira de Física* **17**, 370 (1987).
- [28] M. Greespan, Rotational relaxation in nitrogen, oxygen, and air, *J. Acoust. Soc. Am.* **31**, 155 (1959).
- [29] W. Marques Jr., Light scattering from extended kinetic models: Polyatomic ideal gases, *Physica A* **264**, 40 (1999).
- [30] A. S. Rana and H. Struchtrup, Thermodynamically admissible boundary conditions for the regularized 13 moment equations, *Phys. Fluids* **28**, 027105 (2016).
- [31] L. Waldmann, Nonequilibrium thermodynamics of boundary conditions, *Z. Naturforsch. A* **22**, 1269 (1967).
- [32] A. S. Rana, V. K. Gupta, and H. Struchtrup, Coupled constitutive relations: A second law based higher-order closure for hydrodynamics, *Proc. R. Soc. London A* **474**, 20180323 (2018).

- [33] S. Kosuge, K. Aoki, M. Bisi, M. Groppi, and G. Martalò, Boundary conditions for two-temperature Navier-Stokes equations for a polyatomic gas, *Phys. Rev. Fluids* **6**, 083401 (2021).
- [34] W. Jitschin and S. Ludwig, Dynamical behaviour of the Pirani sensor, *Vacuum* **75**, 169 (2004).
- [35] S. J. O'shea and R. E. Collins, An experimental study of conduction heat transfer in rarefied polyatomic gases, *Int. J. Heat Mass Transf.* **35**, 3431 (1992).
- [36] P. J. Sun, J. Y. Wu, P. Zhang, L. Xu, and M. L. Jiang, Experimental study of the influences of degraded vacuum on multilayer insulation blankets, *Cryogenics* **49**, 719 (2009).
- [37] Y. Yang, I. Gerken, J. J. Brandner, and G. L. Morini, Design and experimental investigation of a gas-to-gas counter-flow micro heat exchanger, *Exp. Heat Transfer* **27**, 340 (2014).
- [38] H. Chalabi, O. Buchina, L. Saraceno, M. Lorenzini, D. Valougeorgis, and G. L. Morini, Experimental analysis of heat transfer between a heated wire and a rarefied gas in an annular gap with high diameter ratio, *J. Phys.: Conf. Ser.* **362**, 012028 (2012).
- [39] S. C. Saxena, Transport properties of gases and gaseous mixtures at high temperatures, *High Temp. Sci.* **3**, 168 (1971).
- [40] F. Sharipov and D. Kalempa, Velocity slip and temperature jump coefficients for gaseous mixtures. iv. temperature jump coefficient, *Int. J. Heat Mass Transf.* **48**, 1076 (2005).
- [41] Yu G Semyonov, S. F. Borisov, and P. E. Suetin, Investigation of heat transfer in rarefied gases over a wide range of Knudsen numbers, *Int. J. Heat Mass Transf.* **27**, 1789 (1984).
- [42] W. M. Trott, J. N. Castañeda, J. R. Torczynski, M. A. Gallis, and D. J. Rader, An experimental assembly for precise measurement of thermal accommodation coefficients, *Rev. Sci. Instrum.* **82**, 035120 (2011).
- [43] H. Yamaguchi, K. Kanazawa, Yu Matsuda, T. Niimi, A. Polikarpov, and I. Graur, Investigation on heat transfer between two coaxial cylinders for measurement of thermal accommodation coefficient, *Phys. Fluids* **24**, 062002 (2012).
- [44] A. Frezzotti, A numerical investigation of the steady evaporation of a polyatomic gas, *Eur. J. Mech. B Fluids* **26**, 93 (2007).
- [45] M. Pavić, T. Ruggeri, and S. Simić, Maximum entropy principle for rarefied polyatomic gases, *Physica A* **392**, 1302 (2013).
- [46] D. C. Gaio and G. M. Kremer, Kinetic theory for polyatomic dense gases of rough spherical molecules, *J. Non-Equilib. Thermodynam.* **16**, 357 (1991).
- [47] V. Djordjic, M. Pavić-Čolić, and M. Torrilhon, A consistent, explicit and accessible Boltzmann collision operator for polyatomic gases, <https://github.com/Boltzmann-polyatomic/Supplements2021> (2021).
- [48] L. Wu and X.-J. Gu, On the accuracy of macroscopic equations for linearized rarefied gas flows, *Adv. Aerodyn.* **2**, 2 (2020).
- [49] C. M. Hammond Jr. and T. A. Wiggins, Rayleigh-Brillouin scattering from methane, *J. Chem. Phys.* **65**, 2788 (1976).
- [50] R. C. Desai and R. Kapral, Translational hydrodynamics and light scattering from molecular fluids, *Phys. Rev. A* **6**, 2377 (1972).
- [51] X.-D. Li, Z.-M. Hu, and Z.-L. Jiang, Continuum perspective of bulk viscosity in compressible fluids, *J. Fluid Mech.* **812**, 966 (2017).
- [52] J. Zhang, P. Luan, J. Deng, P. Tian, and T. Liang, Theoretical derivation of slip boundary conditions for single-species gas and binary gas mixture, *Phys. Rev. E* **104**, 055103 (2021).
- [53] C. Tantos, D. Valougeorgis, and A. Frezzotti, Conductive heat transfer in rarefied polyatomic gases confined between parallel plates via various kinetic models and the dsmc method, *Int. J. Heat Mass Transf.* **88**, 636 (2015).
- [54] S. Busto, M. Dumbser, I. Peshkov, and E. Romenski, On thermodynamically compatible finite volume schemes for continuum mechanics, *SIAM J. Sci. Comput.* **44**, A1723 (2022).
- [55] A. S. Rana, S. Saini, S. Chakraborty, D. A. Lockerby, and J. E. Sprittles, Efficient simulation of nonclassical liquid–vapor phase-transition flows: A method of fundamental solutions, *J. Fluid Mech.* **919**, A35 (2021).
- [56] Himanshi, A. S. Rana, and V. K. Gupta, Fundamental solutions of an extended hydrodynamic model in two dimensions: Derivation, theory, and applications, *Phys. Rev. E* **108**, 015306 (2023).
- [57] A. S. Rana and S. Barve, A second-order constitutive theory for polyatomic gases: Theory and applications, *J. Fluid Mech.* **958**, A23 (2023).